

# Application of Aerial InSAR to Measure Glacier Elevations

Bryce Glenn<sup>1</sup>, Andrew G. Fountain<sup>1</sup>, and Delwyn Moller<sup>2</sup>

<sup>1</sup>Portland State University

<sup>2</sup>University of Auckland

March 9, 2023

## Abstract

Glaciers and perennial snowfields are important to alpine ecosystems and regional hydrology. Quantifying volume change of a population of glaciers widely distributed over a region is difficult and expensive. We employed NASA's novel Airborne Glacier and Ice Surface Topography Interferometer (GLISTIN) to rapidly map surface topography of alpine glaciers across the western USA. In five flight days 3289 glaciers and perennial snowfields were surveyed. Comparison with lidar over control sites showed a mean difference of  $+0.17 \pm 1.78$  m at a spatial scale of 3 m. Data coverage increased and elevation uncertainty decreased with the mosaicking of multiple passes due to the complex terrain. Elevation change since the National Elevation Dataset shows a thinning (and volume loss) over the last ~56 years, averaging  $-0.3 \pm 0.2$  m and accelerating since 1980. GLISTIN can be a valuable tool for rapidly mapping ice surfaces in the alpine environment.

1  
2                   **Application of Aerial InSAR to Measure Glacier Elevations**

3  
4                   **Bryce Glenn<sup>1</sup>, Andrew G. Fountain<sup>1</sup>, Delwyn Moller<sup>2</sup>**

5  
6                   <sup>1</sup> Department of Geology, Portland State University, Portland, Oregon, USA 97207

7                   <sup>2</sup> Department of Electrical, Computer & Software Engineering, University of Auckland,  
8                   Auckland, New Zealand

9  
10                   Corresponding author: Andrew G. Fountain, [andrew@pdx.edu](mailto:andrew@pdx.edu)

11  
12  
13                   **Key Points:**

- 14                   • Aerial InSAR can rapidly map the topography of alpine glaciers over a broad  
15                   region.
- 16                   • Elevations compare favorably to lidar,  $+0.17 \pm 1.78$  m at spatial scale of 3 m.
- 17                   • The mean rate of glacier elevation change (specific volume) is  $-0.3 \pm 0.2$  m yr<sup>-1</sup>  
18                   for the past 56 years with rates increasing since 1980.

19  
20

21 **Abstract**

22

23 Glaciers and perennial snowfields are important to alpine ecosystems and regional  
24 hydrology. Quantifying volume change of a population of glaciers widely distributed  
25 over a region is difficult and expensive. We employed NASA's novel Airborne Glacier  
26 and Ice Surface Topography Interferometer (GLISTIN) to rapidly map surface  
27 topography of alpine glaciers across the western USA. In five flight days 3289 glaciers  
28 and perennial snowfields were surveyed. Comparison with lidar over control sites showed  
29 a mean difference of  $+0.17 \pm 1.78$  m at a spatial scale of 3 m. Data coverage increased  
30 and elevation uncertainty decreased with the mosaicking of multiple passes due to the  
31 complex terrain. Elevation change since the National Elevation Dataset shows a thinning  
32 (and volume loss) over the last ~56 years, averaging  $-0.3 \pm 0.2$  m and accelerating since  
33 1980. GLISTIN can be a valuable tool for rapidly mapping ice surfaces in the alpine  
34 environment.

35

36 **Plain Language Summary**

37

38 Glaciers and perennial snowfields are important water sources to alpine ecosystems and  
39 regional hydrology. To quantify their contribution their volume change is measured by  
40 mapping elevation changes of the ice surface. However, quantifying volume change for a  
41 population of glaciers widely distributed over a region is difficult and expensive. We  
42 employed NASA's airborne radar (GLISTIN) to rapidly map surface topography of  
43 alpine glaciers across the western USA. In only five flight days 3289 glaciers and  
44 perennial snowfields were surveyed. GLISTIN data over control-regions were compared  
45 to lidar, an independent elevation measure using lasers, and showed small differences  
46 indicating this method can be a valuable and cost-effective tool to track glacier change in  
47 the future. Comparing the new elevations against historic elevations from USGS maps a  
48 dramatic thinning (and volume loss) over the last ~60 years.

49

50 **1. Introduction**

51

52 Glacier melt is important to runoff in high alpine landscapes. At a local scale, melting  
53 glaciers maintain streamflow during the dry, late summer months after the seasonal snow

54 has melted (Fountain & Tangborn, 1985; Moore et al., 2009). Shrinking glaciers lose ice  
55 volume and supply more water to streams and rivers than anticipated from precipitation.  
56 Although this may be a temporary benefit, particularly in dry regions, their ability to  
57 buffer seasonal runoff in future is reduced, making watersheds more vulnerable to  
58 drought (Hall & Fagre, 2003; Moore et al., 2009). At a global scale, mass transfer of  
59 water from storage as ice to water runoff increases global sea-levels (Meier, 1984; Pfeffer  
60 et al., 2014; Zemp et al., 2019).

61

62 Traditionally, tracking glacier mass change was a field effort based on measuring the gain  
63 and loss of snow and ice at points on the glacier (Kaser et al., 2003; Ostrem & Brugman,  
64 1991). Although these efforts produce high-quality results showing spatial variations in  
65 mass change across a glacier only a few glaciers can be so monitored by any agency  
66 (Andreassen et al., 2005; O’Neel et al., 2019). Remote-sensing methods can be used to  
67 cover broad regions using an alternative approach that estimates mass change from  
68 volume change. Differential interferometric synthetic aperture radar (InSAR) can map  
69 surface elevation changes and offers the advantage of an all-weather, day/night  
70 capability, a particularly valuable tool in often cloudy alpine environments (Rosen et al.,  
71 2000). Satellite-borne applications have revolutionized our understanding of Antarctica  
72 and Greenland (Mouginot et al., 2019; Shepherd et al., 2018), and more recently, the  
73 larger alpine glaciers (Millan et al., 2022). Challenges using InSAR include shadowing,  
74 decorrelation due to layover, phase unwrapping, and temporal landscape changes  
75 (Eineder & Holzner, 2000; Rees, 2000).

76

77 Here, we test a novel approach for determining surface elevations on alpine glaciers using  
78 an airborne single-pass InSAR, NASA’s Glacier, and Ice Surface Topography  
79 Interferometer (GLISTIN; Moller et al., 2017). Unlike differential/repeat-pass InSAR,  
80 GLISTIN collects two radar images simultaneously, allowing elevations to be derived  
81 from a single flight pass and are thus not sensitive to temporal decorrelation between  
82 observations. Mounted on a jet aircraft, GLISTIN can image large areas in a short time  
83 and has been used to map the relatively gentle topography of large glaciers and ice sheets

84 (Hensley et al., 2016; Moller et al., 2019). We evaluate its performance to map small  
85 alpine glaciers in complex terrain across a broad region. In addition, the updated glacier  
86 elevations are differenced from the National Elevation Data (Gesch, 2002) to calculate  
87 glacier elevation change across the western US.

88

## 89 **2. Data and Methods**

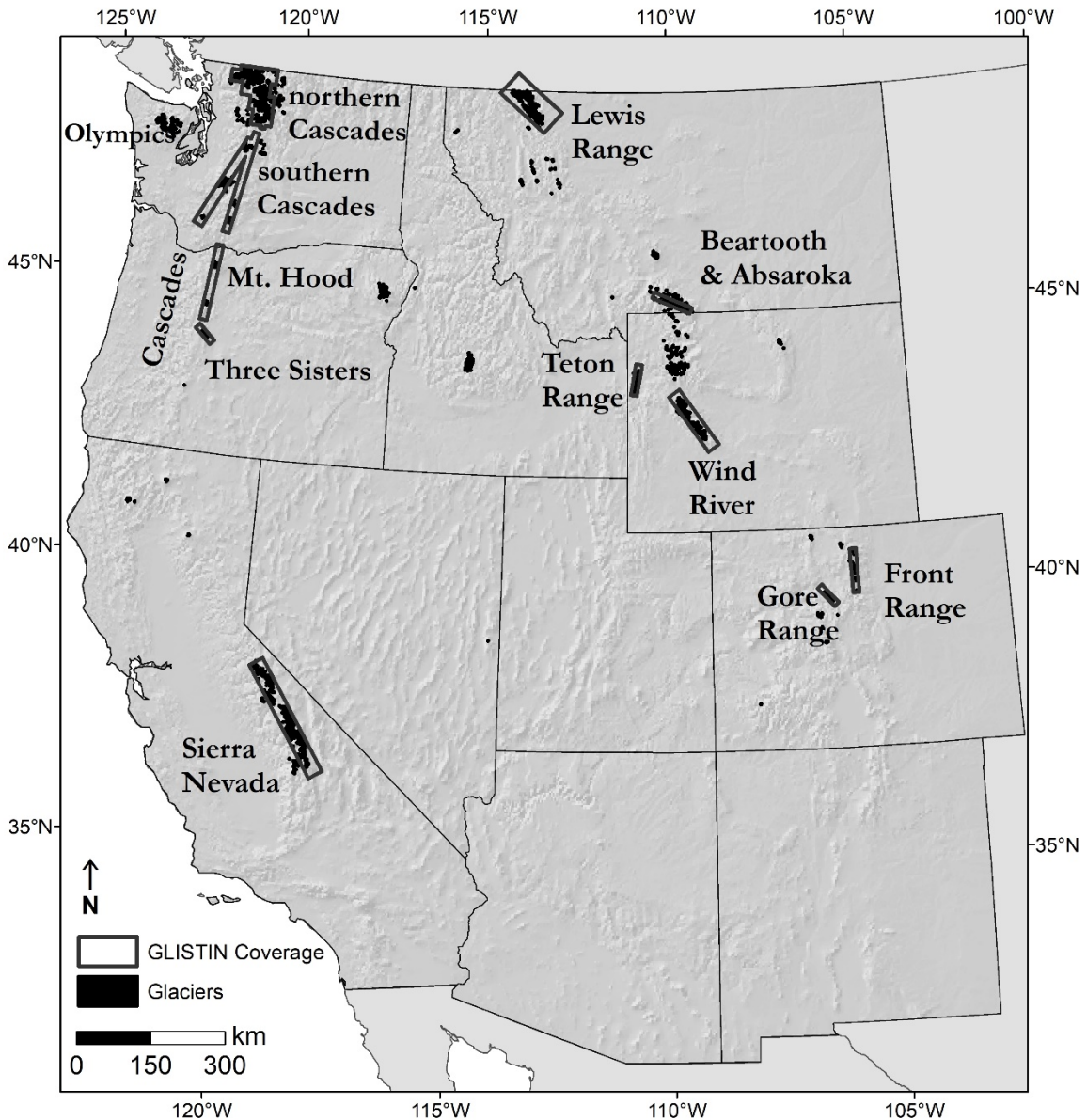
90

### 91 2.1 Study Area

92

93 The study region is the American West, defined as the continental United States west of  
94 the 100th meridian enclosing about  $2 \times 10^6$  km<sup>2</sup> and home to about 5036 glaciers and  
95 perennial snowfields ( $\geq 0.01$  km<sup>2</sup>) as of the late 20<sup>th</sup> century (Figure 1; Fountain et al.,  
96 2017). The region is made up of three large mountain ranges, the Rocky Mountains, the  
97 Cascade Range, and the Sierra Nevada. Many peaks exceed 4000 m in. The largest  
98 concentration of glaciers, and lowest elevation (2000 m - 3000 m asl) is in the maritime  
99 climate of the Pacific Northwest (Oregon, Washington, north-west Montana,). The  
100 remaining glaciers are in continental climates elsewhere at high elevations, > 3000m.

101



102  
 103 **Figure 1.** Map of glaciers and perennial snowfields (black dots) in the Western U.S. The  
 104 boxes show regions surveyed by GLISTIN.

105  
 106 Regional studies have shown drastic decreases in glacier area exceeding 50% over the  
 107 last century (DeVisser & Fountain, 2015; Fagre et al., 2017; O’Neal et al., 2019). The  
 108 rate of change has not been constant or spatially uniform (Basagic & Fountain, 2011;  
 109 Hoffman et al., 2007; O’Neal et al., 2015). Glacier volume changes, estimated by  
 110 differencing topography over time, show a loss on Mount Rainier, WA, of  $-0.65 \text{ km}^3$ ,

111 average specific mass loss rate of  $-0.16 \text{ m w.e yr}^{-1}$  (1970 - 2007/2008; Sisson et al.,  
112 2011). Menounos et al. (2018) estimated a volume loss of  $-127.65 \pm 45.17 \text{ km}^3$ ,  $-0.42 \pm$   
113  $0.15 \text{ m w.e.}$  between 2000 and 2018 for most of the glaciated terrain in Western North  
114 America.

## 115 116 2.2 GLISTIN

117  
118 GLISTIN is a Ka-band radar (8.4 mm, 35.66 GHz) system that utilizes two horizontally  
119 polarized antennas, 0.25 m apart in elevation, both of which are capable of transmitting  
120 and receiving (Moller et al., 2019). Unlike repeat-pass InSAR, GLISTIN's dual antennas,  
121 collect data simultaneously. The Ka-band center frequency enables high accuracy with a  
122 compact architecture and reduces snow penetration compared to lower frequencies. This  
123 cross-track InSAR system is capable of providing not only the position of each image  
124 point in along-track and slant range as with traditional SAR but also the height of that  
125 point via the interferometric phase. Because the phase repeats after  $2\pi$ , it must be  
126 "unwrapped" to determine its unique location and height relative to a reference surface  
127 (Moller et al., 2011; Rosen et al., 2000). The system is contained in an external pod  
128 beneath NASA's Gulfstream-III aircraft with left looking view angles of  $15\text{-}50^\circ$  from  
129 nadir. The system is coupled to inertial navigation and global position that provide pitch  
130 and roll of the aircraft as well as its precise position in space. Nominal flight altitudes are  
131 about 12,500 m above sea-level with a ground swath width of about 12 km and its typical  
132 air speed is  $720 \text{ km hr}^{-1}$ .

133  
134 To guide the aerial survey, the locations of the glaciers were retrieved from Fountain et  
135 al. (2017). Flight passes were typically flown in pairs, each in an opposite direction, to  
136 reduce gaps in backscatter from radar shadow or layover in the mountainous terrain. In a  
137 few regions additional perpendicular flight passes were also flown. The georectified  
138 height-maps from each pass were mosaicked into a 3-meter pixel-size digital elevation  
139 model (DEM; Hensley et al., 2016) and projected into the Universal Transverse Mercator  
140 (UTM) coordinate system. Self-reported elevation accuracy is 'height-precision', a  
141 statistical estimate based on the interferometric correlation of each individual radar pixel

142 making up the 3 m mosaicked pixel (Moller et al., 2011). In the final mosaicked DEM,  
143 the elevation of each pixel is the weighted sum of elevations from individual passes and  
144 the weights are inversely proportional to the height-precision (Hensley et al., 2016). The  
145 vertical absolute uncertainty of GLISTIN-derived topography was found to be about  $\pm$   
146 0.30 m over bare non-snow-covered terrain (Schumann et al., 2016). Data collection and  
147 processing were provided by the Jet Propulsion Laboratory at California Institute of  
148 Technology, Pasadena, CA.

### 149 150 2.3 Accuracy

151  
152 The accuracy of GLISTIN elevations was ground-truthed by differencing lidar DEMs  
153 from GLISTIN DEMs (Table SOM2). All lidar data were converted from its native  
154 coordinate system to WGS84 to UTM using Vdatum (Version 3.8, 2017, National  
155 Oceanic and Atmospheric Administration, Washington, DC), inducing an error of about  
156 0.076 m (self-reported by Vdatum during conversion) and resampled to 3 m to match the  
157 GLISTIN DEMs spatial posting, using bilinear interpolation. To calculate elevation  
158 change the  $\frac{1}{3}$  arc-second NED was converted to UTM (WGS84) using Vdatum and  
159 resampled to 10 m using bilinear interpolation. GLISTIN and lidar elevations were also  
160 resampled to 10 m using bilinear interpolation to match the NED. The relative accuracy  
161 of GLISTIN, lidar, and the NED were inter-compared at four barren earth snow-free  
162 control zones in the Cascade Range of Oregon and Washington where all three estimates  
163 of elevation were available. Each control zone is a patchwork of co-located but isolated  
164 terrains. Barren earth terrains were derived from the 'barren' class of the 2016 National  
165 Land Cover Database (<https://www.mrlc.gov/data/nlcd-2016-land-cover-conus>).  
166 GLISTIN's performance imaging ice/snow surfaces was examined by comparing  
167 elevations to lidar data acquired on Mount Adams, Washington, which was flown 28  
168 days prior to the GLISTIN flights. We expect GLISTIN to yield somewhat lower  
169 elevations due to melting of the snow and ice.

170  
171  
172



173 2.4 Area and Volume Change

174

175 The reference area and elevation of the glaciers and perennial snowfields are derived  
176 from (Fountain et al., 2017) and a ‘historic’ version of the NED (Gesch et al., 2002),  
177 respectively. Both are based on the original U.S. Geological Survey 1:24000 topographic  
178 maps from which the glacier outlines and elevations were derived. The maps in the  
179 western US were drawn over a period of years (1940s-1980s. Resolution of the NED is  $\frac{1}{3}$   
180 arc-second ( $\sim 10$  m), and the horizontal and vertical coordinate systems are North  
181 American Datum of 1983, North American Vertical Datum of 1988, respectively. The  
182 NED is continually being updated and it was necessary to retrieve the original ‘historic’  
183 version from multiple sources (Table SOM1).

184

185 Volume change was estimated by differencing the GLISTIN elevations from the NED  
186 elevations within the original perimeter and for only those glaciers with  $\geq 80\%$  GLISTIN  
187 coverage. Le Bris and Paul (2015) showed that good estimates of volume change can be  
188 achieved with the elevation postings cover at least 80% of the glacier area. Reasonable  
189 estimates of volume change can be obtained for coverages as low as 40%, however  
190 results depend on interpolation method (McNabb et al., 2019), so we adopted the more  
191 conservative threshold of 80% used by Le Bris and Paul (2015). In order to compare  
192 volume loss between large and small glaciers and because the historic mapping occurred  
193 over a time-span of decades across the western US, results are expressed as the rate of  
194 specific volume (volume/area) change ( $\text{m}^{-3} \text{m}^{-2} \text{yr}^{-1}$  or  $\text{m} \text{yr}^{-1}$ ).

195

196 Uncertainty of volume change,  $\sigma_{\Delta V}$ , is calculated for each individual glacier or perennial  
197 snowfield, using the vertical and area uncertainties (Menounos et al., 2018),

198 
$$\sigma_{\Delta V} = \sqrt{(\sigma_{\Delta z} A_g)^2 + (\sigma_A \Delta z)^2}, \quad (1)$$

199

200 where  $\sigma_{\Delta z}$  is the RMSE of elevation differences between GLISTIN and the NED for all  
201 barren earth control zones, for the region in which the glacier or perennial snowfield is  
202 located,  $A_g$  is the original (historic) area of the glacier or perennial snowfield,  $\Delta z$  is the

203 average elevation change of the glacier or perennial snowfield, and  $\sigma_A$  is area uncertainty.  
204 Uncertainty of the original areas is considered 9% (Fountain et al., 2017).

205

### 206 3. Results and Analysis

207

#### 208 3.1 Data collection

209

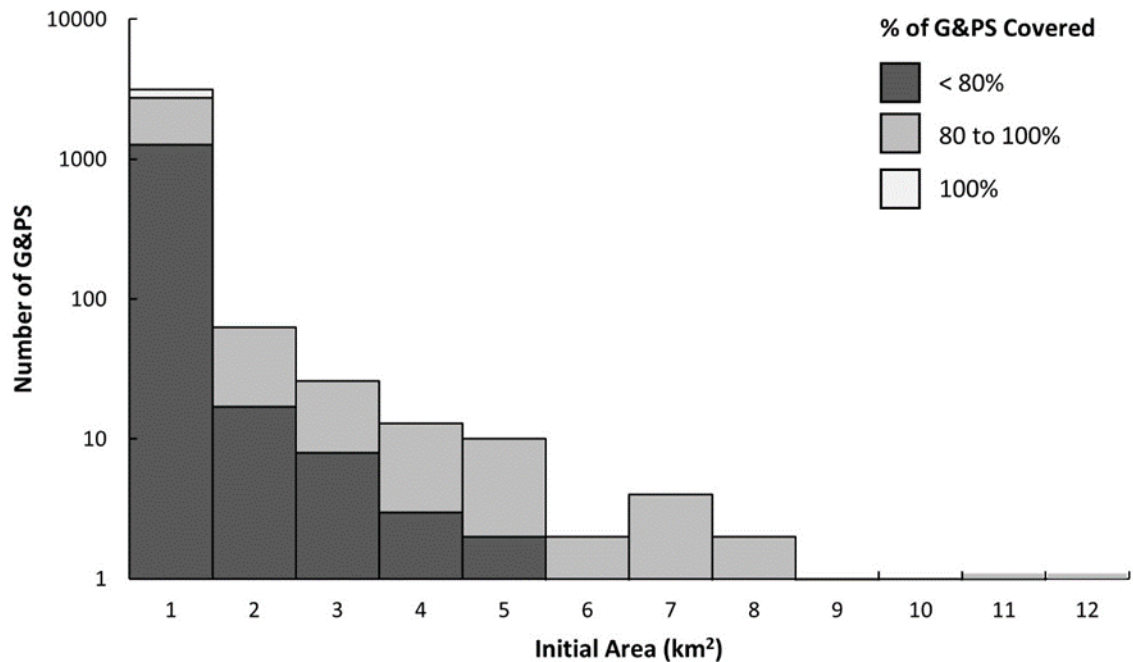
210 The GLISTIN flights imaged the glacier-populated mountains of the American West for  
211 5 flight days, between September 12 to 28, 2016, covering about 41,000 km<sup>2</sup> (Figure 1).

212 Due to an unexpected reassignment of the aircraft, several mountain ranges were not  
213 included, most notably the Olympic Mountains, WA, and the Absaroka Range, WY.

214 Within the regions surveyed 3889 glaciers and perennial snowfields are present.

215 GLISTIN coverage of each varied from 0 to 100% with a median of 81%. The total  
216 number of features with  $\geq 80\%$  coverage was 1770 (309 km<sup>2</sup>, 53% of the total area of  
217 surveyed G&PS; figure 2).

218



219

220 **Figure 2.** Histogram of the initial area of glaciers and perennial snowfields and the

221 fraction of area mapped by GLISTIN. Initial area refers to the area from the U.S.

222 Geological Survey's 1:24000 map series. The x-axis value is the maximum for each bin.

223

224

225 As expected, increasing the number of flight passes over the same area increased the  
226 backscatter coverage. For one flight pass backscatter was received from 17% of the entire  
227 illuminated area, for two flights 66%, four flights, 86%, and for eight flights 94% (Table  
228 SOM3). No significant difference was observed in backscatter coverage of snow/ice  
229 surfaces compared to ice-free surfaces, and within glaciers no significant differences  
230 between snow-covered regions and ice-exposed regions. Backscatter reception was only  
231 significantly correlated with terrain slope with greater loss on steeper slopes.

232

### 233 3.2 Accuracy

234

235 The GLISTIN DEMs for three of the four barren earth control zones were compiled from  
236 multiple passes. The fourth control zone (Mount Adams, WA) was comprised of single  
237 pass data and was examined separately. For the three multi-pass barren earth control  
238 zones the GLISTIN – lidar (3 m posting) mean difference was  $+0.17 \pm 1.78$  m (Table  
239 SOM4). Comparing GLISTIN and the NED over the same regions (10 m posting), the  
240 mean difference and standard deviation was much larger,  $+1.05 \pm 6.38$  m. This is due to  
241 the much larger uncertainty in the NED elevations of 3.74 m, which is based mostly on  
242 control points located in lower elevation and less complex terrain (Gesch, 2007). The  
243 mean lidar-NED difference  $-0.89 \pm 5.83$ , supports this inference. For the control zones on  
244 Mount Adams, the mean elevations difference of single-pass GLISTIN - lidar (3 m  
245 posting) was  $-0.00 \pm 3.20$  m, whereas for the snow/ice surfaces it was  $-0.86 \pm 3.76$  m.  
246 The negative difference for the snow/ice surfaces is to be expected given the melting that  
247 occurred over the 28-day period between the initial lidar survey followed by the  
248 GLISTIN survey. Given that the snow is wet during this time of year and interferometric  
249 penetration is negligible (Hensley et al., 2016).

250 With respect to interferometric radar errors it is important to note that the height precision  
251 is dominated by the instrument random noise. This relative error is high frequency and  
252 will scale with spatial averaging of uncorrelated pixels or independent samples. The  
253 same is not true for the height accuracy or systematic (mean) offset which does not

254 improve with averaging as they are correlated. Therefore, if we calculate the RMSE for  
255 more coarse spatial postings this metric will reduce significantly (with the random  
256 /precision inversely proportional to the square-root of the effective number of  
257 independent looks (Hensley et. al. 2016). For this paper we analyze GLISTIN data at a  
258 spatial posting of 3m due to the small footprint of many of these glaciers. However, one  
259 can expect significantly improved height precision, and thereby RMSE for large glaciers  
260 via spatial averaging. The low mean difference (i.e. accuracy) observed for the barren  
261 areas indicates that extremely low height errors are achievable with sufficient spatial  
262 averaging to reduce the random component (Schumann et. al. 2016; Moller et.al. 2019)

263 Although no correlation was observed between mean elevation difference (GLISTIN -  
264 lidar) and surface slope, the standard deviation increased from about 1.7 m for slopes  
265 between 20° and 30° to 3.8 m for slopes between 50° and 60°. The RMSE (GLISTIN-  
266 NED) increased from 6.1 m for slopes 20° to 30° to 10.2 m for slopes between 50° and  
267 60°. The rate of phase change is a function of the interferometric measurement geometry  
268 and is directly proportional to the local slope. Phase unwrapping becomes more difficult  
269 as the slope increases so an increased RMSE in extreme topography is to be expected.  
270 The orientation of single-pass GLISTIN relative to the terrain surface affects the  
271 elevation difference. The mean elevation difference (GLISTIN-lidar) was smaller for  
272 surfaces facing towards GLISTIN,  $+0.01 \pm 2.07$  m, than surfaces facing away,  $+0.07 \pm$   
273  $4.03$  m.

### 274 3.3 Volume change

275  
276 Volume change was estimated for 1770 glaciers and perennial snowfields (54% of total)  
277 consisting of 351 glaciers and 1419 snowfields. Overall mean uncertainty, based on  
278 barren earth control zones across the west (Table SOM5), was  $-0.37 \pm 7.31$  m. Rejecting  
279 those specific volume changes that were smaller than uncertainty yielded 231 glaciers  
280 totaling  $198.84 \text{ km}^2$  and 551 perennial snowfields ( $21.31 \text{ km}^2$ ). Comparing our volume  
281 change to a prior estimate for Mt. Rainier, Washington (Sisson et al., 2011), showed that  
282 the prior estimate, based on a lidar-NED difference, of  $-8.6$  m (1970-2007) is within the

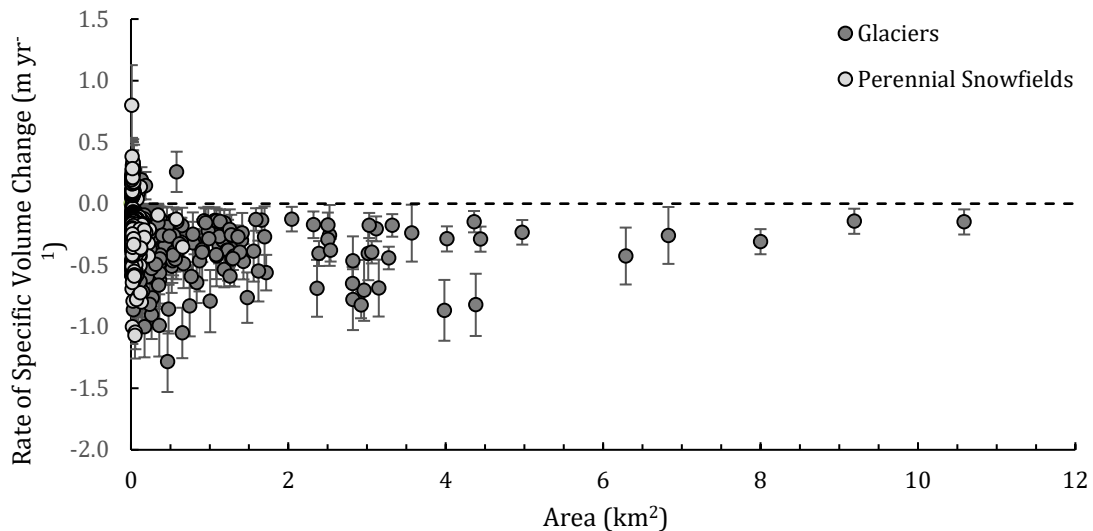
283 uncertainty of our value ,  $-9.7 \pm 4.8$  m (1970-2016). That our estimate showed a greater  
284 mass loss is consistent with the longer time period of comparison.

285

286 Most glaciers and perennial snowfields lost mass (Figure 3). The median rate of change  
287 for glaciers,  $-0.3 \pm 0.2$  m yr<sup>-1</sup>, and for snowfields,  $-0.2 \pm 0.2$  m yr<sup>-1</sup>. Four glaciers (2%)  
288 and 56 (10%) perennial snowfields increased in volume; their locations are not region  
289 specific. These features are characterized by small area, median 0.02 km<sup>2</sup> (all but one <  
290 0.2 km<sup>2</sup>), steeper slopes, and higher elevations. The features that gained volume were at  
291 significantly higher elevations and steeper slopes (median 3100 m, 28°) compared to  
292 those that lost volume, (median 2335 m 25°;  $p < 0.05$ , Mann-Whitney U). The time series  
293 of ice mass loss in the Cascade Range, Washington is relatively complete compared to  
294 other regions and show increasing mass loss with time (Figure 4). The rate of change  
295 increased significantly since 1980.

296

297



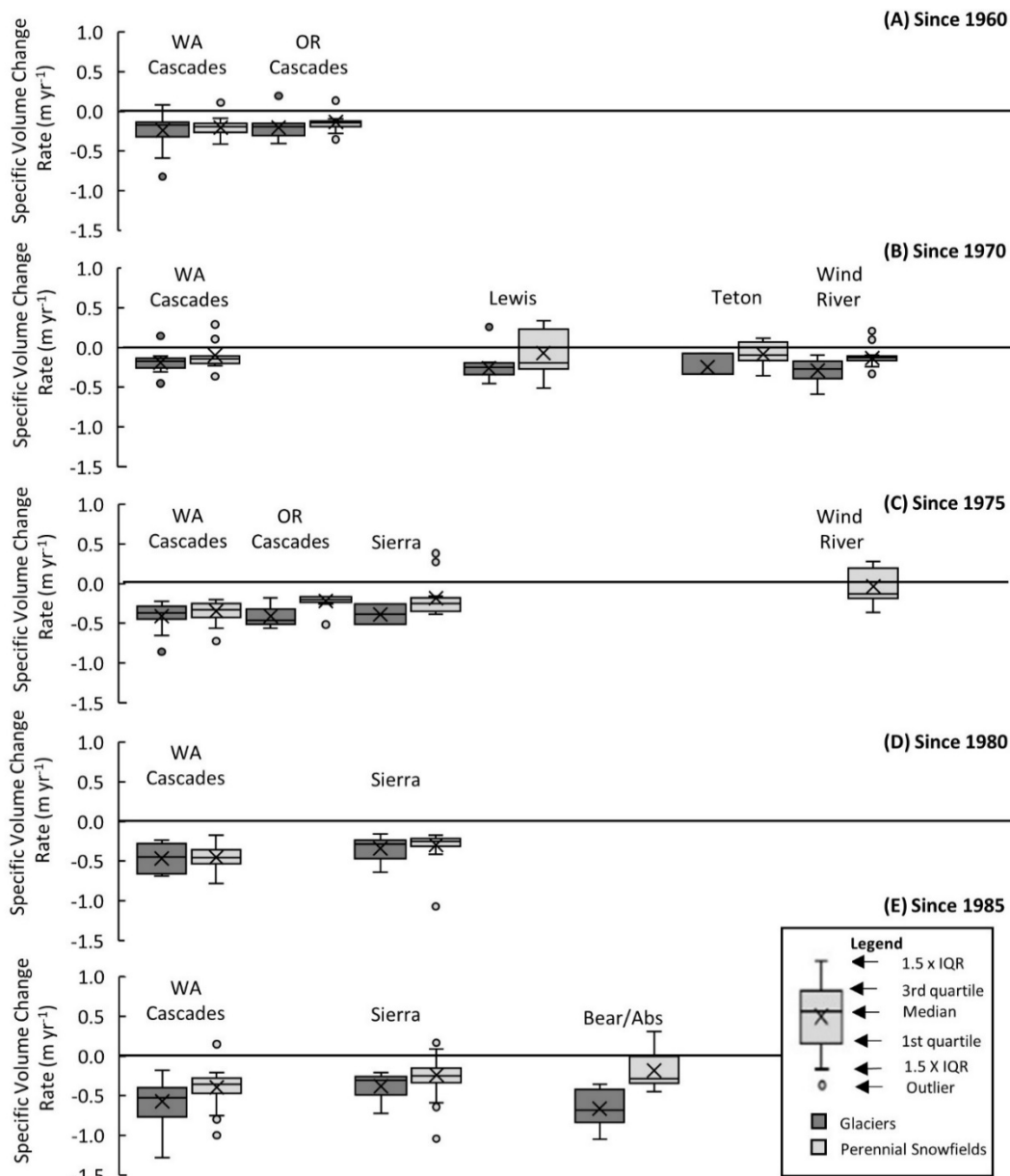
298

299 **Figure 3.** Specific volume change of glaciers and perennial snowfields (G&PS). Light  
300 grey circles represent perennial snowfields, and dark grey circles represent glaciers. The  
301 ‘whiskers’ represent uncertainty. Initial area refers to the area from the U.S. Geological  
302 Survey’s 1:24000 map series.

303

304

305  
306



307  
308

309 **Figure 4.** Volume change glaciers (dark grey boxes) and perennial snowfields (light grey  
310 boxes) for each region with more than ten features, grouped by initial mapping date (all  
311 ending in 2016), 1960 (1956 to 1960) (A), 1970 (1966 to 1970) (B), 1975 (1971 to 1975)  
312 (C), 1980 (1976 to 1980) (D), and 1985 (1981 to 1985) (E). The ‘whiskers’ represent the  
313 smallest and largest values not considered outliers. The values that exceed 1.5 times the  
314 interquartile range (IQR) below the first quartile or above the third quartile are  
315 considered outliers (open circles ‘Bear/Abs’ refers to Beartooth-Absaroka, MT).

316

#### 317 **4. Discussion and Conclusions**

318

319 GLISTIN was developed for measuring the relatively flat surfaces of large glaciers and  
320 ice sheets, and its application to the complex topography alpine terrain presents a stress-  
321 case for the instrument. GLISTIN elevation mosaics compared favorably to lidar  
322 measurements over barren earth  $+0.17 \pm 1.78$  m (3 m posting). Similar comparisons over  
323 bedrock in Greenland showed,  $+0.32 \pm 0.95$  m (30 m posting) for single pass elevations  
324 (Moller et al., 2019). Over snow and ice surfaces on Mount Adams the mean difference  
325 of GLISTIN and lidar was  $-0.87 \pm 3.8$  m (3 m posting). We regard much of the difference  
326 due to snow and ice melt over the 28-day interval between the initial lidar and later  
327 GLISTIN surveys. Similar mean GLISTIN – lidar differences, were observed on two  
328 gently sloping glacier surfaces in Alaska,  $+0.8 \pm 1.7$  m and  $+1.2 \pm 3.7$  m (3 m posting,  
329 Moller et al., 2019). There was a similarly substantial time interval between the GLISTIN  
330 and subsequent lidar surveys of 1.5 month and 1 month, respectively. Differencing  
331 GLISTIN from the NED for estimating historic glacier change showed the RMSE at  
332 control zones to be 7.35 m and largely driven by uncertainty in the NED.

333

334 The standard deviations for all elevation comparisons increased with surface slope and  
335 most likely due to small offsets in aligning the DEMs. This result is also common to  
336 other studies using matching DEMs. The mean elevation difference (Shuttle Radar  
337 Topography Mission 1 Arc-Second Global DEM) over non-glaciated terrain near the  
338 Akshirak glaciers (Tien Shan, Central Asia) was  $-4.5 \pm 10.9$  m for slopes between  $25^\circ$   
339 and  $30^\circ$ , increasing to  $-7.6 \pm 25.6$  m for slopes between  $40^\circ$  and  $78^\circ$  (Paul, 2008;  
340 Surazakov & Aizen, 2006). For North & Middle Sisters, Oregon the RMSE (lidar-NED)  
341 was 5.7 m and 12.3 m for slopes between  $20^\circ$  to  $30^\circ$  and  $50^\circ$  to  $60^\circ$ , respectively  
342 (Ohlschlager, 2015), and similar to the GLISTIN-NED RMSE of 6.4 m and 10.2 m for  
343 the same slope bins.

344

345 Elevations were acquired for 85% of the surveyed glaciers and perennial snowfields, of  
346 which 12% were completely mapped and 60% had  $\geq 80\%$  coverage. Increased number of

347 flight passes increased data coverage. This is one clear advantage over satellite InSAR  
348 that look direction can be easily changed. Most of the missing backscatter was caused by  
349 radar shadow and some from layover due to the steep terrain.

350

351 Rates of glacier specific mass loss across the western US are consistent with rates  
352 estimated by other studies in our region. Overall, our rates over the last period of our  
353 study 1985 - 2016 are consistent with the western US average (2000-2020) of about  $-0.4$   
354  $\text{m yr}^{-1}$  (Hugonnet et al., 2021). For the Cascade Range in Washington, Menounos et al.  
355 (2018) estimated  $-0.29 \pm 0.10 \text{ m yr}^{-1}$  (2000-2018) from DEMs derived from optical  
356 satellite imagery, which is half of our estimate of  $-0.63 \pm 0.26 \text{ m yr}^{-1}$  over the longer time  
357 period of 1985-2016. Furthermore, our historic (pre-2000) rates of change is similar to  
358 rates elsewhere globally (Andreassen et al., 2020; Carturan et al., 2013; DeBEER &  
359 Sharp, 2007; Lambrecht & Kuhn, 2007). We also note an acceleration in mass loss since  
360 1980.

361

362 GLISTIN makes an important contribution in tracking glacier change because data can be  
363 rapidly collected unimpeded by weather providing a near instantaneous elevation survey  
364 of glaciers across broad regions. It performed well in complex terrain exceeding its  
365 design requirement and future improvements in flight planning will reduce the  
366 uncertainty. Significantly improved uncertainty for larger glaciers is expected due to  
367 spatial averaging that reduces the random error component.

368

### 369 **Acknowledgments**

370 This work was supported by NASA grant NNX17AI59G. The authors would like to  
371 thank Yang Zhen and the GLISTIN group at JPL for their help in data processing and  
372 interpretation.

### 373 **Data Availability Statement**

374 Analyzed data are included as Supporting Information S1. The single radar swaths of  
375 elevation can be obtained from NASA, <https://uavsar.jpl.nasa.gov/cgi-bin/data.pl>, select



376 TopSAR (Ka-band). The mosaicked radar swaths used in this study can be found at,  
377 [https://pdxscholar.library.pdx.edu/geology\\_data/5/](https://pdxscholar.library.pdx.edu/geology_data/5/). The reference glacier outlines and  
378 elevations derived from the historic 1:24,000 USGS topographic maps and historic  
379 National Elevation Dataset (NED), respectively are located at,  
380 [https://pdxscholar.library.pdx.edu/geology\\_data/4/](https://pdxscholar.library.pdx.edu/geology_data/4/) .

381

## 382 **References**

- 383 Andreassen, L. M., Elvehøy, H., Kjøllmoen, B., & Belart, J. M. C. (2020). Glacier  
384 change in Norway since the 1960s – an overview of mass balance, area, length  
385 and surface elevation changes. *Journal of Glaciology*, *66*(256), 313–328.  
386 <https://doi.org/10.1017/jog.2020.10>
- 387 Andreassen, L. M., Elvehøy, H., Kjøllmoen, B., Engeset, R. V., & Haakensen, N. (2005).  
388 Glacier mass-balance and length variation in Norway. *Annals of Glaciology*, *42*,  
389 317–325. <https://doi.org/10.3189/172756405781812826>
- 390 Basagic, H. J., & Fountain, A. G. (2011). Quantifying 20th Century Glacier Change in  
391 the Sierra Nevada, California. *Arctic, Antarctic, and Alpine Research*, *43*(3), 317–  
392 330. <https://doi.org/10.1657/1938-4246-43.3.317>
- 393 Carturan, L., Filippi, R., Seppi, R., Gabrielli, P., Notarnicola, C., Bertoldi, L., Paul, F.,  
394 Rastner, P., Cazorzi, F., Dinale, R., & Dalla Fontana, G. (2013). Area and volume  
395 loss of the glaciers in the Ortles-Cevedale group (Eastern Italian Alps): Controls  
396 and imbalance of the remaining glaciers. *The Cryosphere*, *7*(5), 1339–1359.  
397 <https://doi.org/10.5194/tc-7-1339-2013>
- 398 DeBEER, C. M., & Sharp, M. J. (2007). Recent changes in glacier area and volume  
399 within the southern Canadian Cordillera. *Annals of Glaciology*, *46*(1), 215–221.  
400 <https://doi.org/10.3189/172756407782871710>
- 401 DeVisser, M. H., & Fountain, A. G. (2015). A century of glacier change in the Wind  
402 River Range, WY. *Geomorphology*, *232*, 103–116.  
403 <https://doi.org/10.1016/j.geomorph.2014.10.017>

404 Eineder, M., & Holzner, J. (2000). Interferometric DEMs in alpine terrain-limits and  
405 options for ERS and SRTM. *IGARSS 2000. IEEE 2000 International Geoscience*  
406 *and Remote Sensing Symposium. Taking the Pulse of the Planet: The Role of*  
407 *Remote Sensing in Managing the Environment. Proceedings (Cat.*  
408 *No.00CH37120)*, 7, 3210–3212 vol.7.  
409 <https://doi.org/10.1109/IGARSS.2000.860385>

410 Fagre, D. B., McKeon, L. A., Dick, K. A., & Fountain, A. G. (2017). *Glacier margin time*  
411 *series (1966, 1998, 2005, 2015) of the named glaciers of Glacier National Park,*  
412 *MT, USA* [Data set]. U.S. Geological Survey. <https://doi.org/10.5066/f7p26wb1>

413 Fountain, A. G., Glenn, B., & Basagic, H. J. (2017). The Geography of Glaciers and  
414 Perennial Snowfields in the American West. *Arctic, Antarctic, and Alpine*  
415 *Research*, 49(3), 391–410. <https://doi.org/10.1657/AAAR0017-003>

416 Fountain, A. G., & Tangborn, W. V. (1985). The effect of glaciers on streamflow  
417 variations. *Water Resources Research*, 21(4), 579–586.

418 Gesch, D., Oimoen, M., Greenlee, S., Nelson, C., Steuck, M., & Tyler, D. (2002). The  
419 national elevation dataset. *Photogrammetric Engineering and Remote Sensing*,  
420 68(1), 5–32.

421 Hall, M. H., & Fagre, D. B. (2003). Modeled climate-induced glacier change in Glacier  
422 National Park, 1850–2100. *BioScience*, 53(2), 131–140.

423 Hensley, S., Moller, D., Oveisgharan, S., Michel, T., & Wu, X. (2016). Ka-Band  
424 Mapping and Measurements of Interferometric Penetration of the Greenland Ice  
425 Sheets by the GLISTIN Radar. *IEEE Journal of Selected Topics in Applied Earth*  
426 *Observations and Remote Sensing*, 9(6), 2436–2450.  
427 <https://doi.org/10.1109/JSTARS.2016.2560626>

428 Hoffman, M. J., Fountain, A. G., & Achuff, J. M. (2007). 20th-century variations in area  
429 of cirque glaciers and glacierets, Rocky Mountain National Park, Rocky  
430 Mountains, Colorado, USA. *Annals of Glaciology*, 46(1), 349–354.  
431 <https://doi.org/10.3189/172756407782871233>

432 Hugonnet, R., McNabb, R., Berthier, E., Menounos, B., Nuth, C., Girod, L., Farinotti, D.,  
433 Huss, M., Dussaillant, I., Brun, F., & Käab, A. (2021). Accelerated global glacier

434 mass loss in the early twenty-first century. *Nature*, 592(7856), 726–731.  
435 <https://doi.org/10.1038/s41586-021-03436-z>

436 Kaser, G., Fountain, A. G., & Jansson, P. (2003). *A manual for monitoring the mass*  
437 *balance of mountain glaciers* (No. 59; IHP-VI Technical Documents in  
438 Hydrology, p. 137). UNESCO.

439 Lambrecht, A., & Kuhn, M. (2007). Glacier changes in the Austrian Alps during the last  
440 three decades, derived from the new Austrian glacier inventory. *Annals of*  
441 *Glaciology*, 46(1), 177–184.

442 Le Bris, R., & Paul, F. (2015). Glacier-specific elevation changes in parts of western  
443 Alaska. *Annals of Glaciology*, 56(70), 184–192.  
444 <https://doi.org/10.3189/2015AoG70A227>

445 McNabb, R., Nuth, C., Käab, A., & Girod, L. (2019). Sensitivity of glacier volume  
446 change estimation to DEM void interpolation. *The Cryosphere*, 13(3), 895–910.  
447 <https://doi.org/10.5194/tc-13-895-2019>

448 Meier, M. F. (1984). Contribution of small glaciers to global sea level. *Science*,  
449 226(4681), 1418–1421.

450 Menounos, B., Hugonnet, R., Shean, D., Gardner, A., Howat, I., Berthier, E., Pelto, B.,  
451 Tennant, C., Shea, J., Noh, M., Brun, F., & Dehecq, A. (2018). Heterogeneous  
452 changes in western North American glaciers linked to decadal variability in zonal  
453 wind strength. *Geophysical Research Letters*.  
454 <https://doi.org/10.1029/2018GL080942>

455 Millan, R., Mouginot, J., Rabatel, A., & Morlighem, M. (2022). Ice velocity and  
456 thickness of the world's glaciers. *Nature Geoscience*, 15(2), 124–129.  
457 <https://doi.org/10.1038/s41561-021-00885-z>

458 Moller, D., Andreadis, K. M., Bormann, K. J., Hensley, S., & Painter, T. H. (2017).  
459 Mapping Snow Depth From Ka-Band Interferometry: Proof of Concept and  
460 Comparison With Scanning Lidar Retrievals. *IEEE Geoscience and Remote*  
461 *Sensing Letters*, 14(6), 886–890.

462 Moller, D., Hensley, S., Mouginot, J., Willis, J., Wu, X., Larsen, C., Rignot, E.,  
463 Muellerschoen, R., & Khazendar, A. (2019). Validation of Glacier Topographic

464 Acquisitions from an Airborne Single-Pass Interferometer. *Sensors*, 19(17), 3700.  
465 <https://doi.org/10.3390/s19173700>

466 Moller, D., Hensley, S., Sadowy, G., Fisher, C., Michel, T., Zawadzki, M., & Rignot, E.  
467 (2011). The Glacier and Land Ice Surface Topography Interferometer: An  
468 Airborne Proof-of-Concept Demonstration of High-Precision Ka-Band Single-  
469 Pass Elevation Mapping. *Geoscience and Remote Sensing, IEEE Transactions*  
470 *On*, 49, 827–842. <https://doi.org/10.1109/TGRS.2010.2057254>

471 Moore, R. D., Fleming, S. W., Menounos, B., Wheate, R., Fountain, A., Stahl, K., Holm,  
472 K., & Jakob, M. (2009). Glacier change in western North America: Influences on  
473 hydrology, geomorphic hazards and water quality. *Hydrological Processes*, 23(1),  
474 42–61. <https://doi.org/10.1002/hyp.7162>

475 Mouginot, J., Rignot, E., Bjørk, A. A., van den Broeke, M., Millan, R., Morlighem, M.,  
476 Noël, B., Scheuchl, B., & Wood, M. (2019). Forty-six years of Greenland Ice  
477 Sheet mass balance from 1972 to 2018. *Proceedings of the National Academy of*  
478 *Sciences*, 116(19), 9239–9244. <https://doi.org/10.1073/pnas.1904242116>

479 Ohlschlager, J. G. (2015). *Glacier Change on the Three Sisters Volcanoes, Oregon:*  
480 *1900–2010* [ProQuest Dissertations Publishing].  
481 <https://search.proquest.com/docview/1718552424?pq-origsite=primo>

482 O’Neal, M. A., Hanson, B., Carisio, S., & Satinsky, A. (2015). Detecting recent changes  
483 in the areal extent of North Cascades glaciers, USA. *Quaternary Research*, 84(2),  
484 151–158. <https://doi.org/10.1016/j.yqres.2015.05.007>

485 O’Neel, S., McNeil, C., Sass, L. C., Florentine, C., Baker, E. H., Peitzsch, E., McGrath,  
486 D., Fountain, A. G., & Fagre, D. (2019). Reanalysis of the US Geological Survey  
487 Benchmark Glaciers: Long-term insight into climate forcing of glacier mass  
488 balance. *Journal of Glaciology*, 65(253), 850–866.  
489 <https://doi.org/10.1017/jog.2019.66>

490 Ostrem, G., & Brugman, M. (1991). *Glacier mass balance measurements: A manual for*  
491 *field and office work* (Science Report No. 4; p. 224). National Hydrology  
492 Research Institute,.

493 Paul, F. (2008). Calculation of glacier elevation changes with SRTM: Is there an  
494 elevation-dependent bias? *Journal of Glaciology*, 54(188), 945–946.

495 Pfeffer, W. T., Arendt, A. A., Bliss, A., Bolch, T., Cogley, J. G., Gardner, A. S., Hagen,  
496 J.-O., Hock, R., Kaser, G., & Kienholz, C. (2014). The Randolph Glacier  
497 Inventory: A globally complete inventory of glaciers. *Journal of Glaciology*,  
498 60(221), 537–552. <https://doi.org/10.3189/2014JoG13J176>

499 Rees, W. G. (2000). Technical note: Simple masks for shadowing and highlighting in  
500 SAR images. *International Journal of Remote Sensing*, 21(11), 2145–2152.  
501 <https://doi.org/10.1080/01431160050029477>

502 Rosen, P. A., Hensley, S., Joughin, I. R., Li, F. K., Madsen, S. N., Rodriguez, E., &  
503 Goldstein, R. M. (2000). Synthetic aperture radar interferometry. *Proceedings of*  
504 *the IEEE*, 88(3), 333–382. <https://doi.org/10.1109/5.838084>

505 Schumann, G. J.-P., Moller, D. K., & Mentgen, F. (2016). High-Accuracy Elevation Data  
506 at Large Scales from Airborne Single-Pass SAR Interferometry. *Frontiers in*  
507 *Earth Science*, 3. <https://doi.org/10.3389/feart.2015.00088>

508 Shepherd, A., Ivins, E., Rignot, E., Smith, B., Van Den Broeke, M., Velicogna, I.,  
509 Whitehouse, P., Briggs, K., Joughin, I., & Krinner, G. (2018). Mass balance of the  
510 Antarctic Ice Sheet from 1992 to 2017. *Nature*, 558, 219–222.

511 Sisson, T. W., Robinson, J. E., & Swinney, D. D. (2011). Whole-edifice ice volume  
512 change AD 1970 to 2007/2008 at Mount Rainier, Washington, based on LiDAR  
513 surveying. *Geology*, 39(7), 639–642.

514 Surazakov, A. B., & Aizen, V. B. (2006). Estimating volume change of mountain glaciers  
515 using SRTM and map-based topographic data. *IEEE Transactions on Geoscience*  
516 *and Remote Sensing*, 44(10), 2991–2995.

517 Zemp, M., Huss, M., Thibert, E., Eckert, N., McNabb, R., Huber, J., Barandun, M.,  
518 Machguth, H., Nussbaumer, S. U., Gärtner-Roer, I., Thomson, L., Paul, F.,  
519 Maussion, F., Kutuzov, S., & Cogley, J. G. (2019). Global glacier mass changes  
520 and their contributions to sea-level rise from 1961 to 2016. *Nature*, 568(7752),  
521 382–386. <https://doi.org/10.1038/s41586-019-1071-0>

522

523 **Supplementary Online Material**

524

525 To identify the date of each glacier DEM, the glacier outlines were combined with a  
526 shapefile of the NED metadata (<https://viewer.nationalmap.gov/basic>) in ArcGIS (ESRI,  
527 Inc.). The NED from non-USGS sources (Table SOM1) did not include metadata for the  
528 imagery date. In those cases, we used the dates listed on the map collars of the USGS  
529 1:24000 topographic maps. Often the same aerial photographs used to create the  
530 topographic maps were also used to derive the NED. Photography used to create the  
531 portion of the NED overlapping the GLISTIN surveys were flown between 1950-1993,  
532 with only two glaciers surveyed in 1950 (Wind River Range, WY) and nine after 1990  
533 (Sierra Nevada, CA). There were 108 glacier outlines where the NED was derived from  
534 imagery spanning multiple years, of which 23 had USGS metadata, clearly identifying  
535 which portion of the outline corresponds with which year. The DEMs covering the  
536 remaining 85 glaciers were from non-USGS sources, and it is unclear what portion of the  
537 glacier were covered by imagery from which year. For G&PS, where multiple images  
538 were used to create the NED, if >80% of the G&PS area was imaged within a single year  
539 (21 G&PS), that year defined the date. For the remaining 64 G&PS, the date is defined as  
540 the average of all years listed. The reported RMSE of the NED (1999 version) is 3.74 m,  
541 but that RMSE under samples high elevation and slopes, fewer than ten samples for slope  
542 > 30°, and ~20 samples for elevations > 3000 m (Gesch, 2007). Therefore, the error over  
543 glaciers and the surrounding alpine environment is probably much higher.

544

545 The NED was split into regions corresponding to the mountain ranges covered by  
546 GLISTIN. In some cases, regions were split into smaller sub-regions to reduce processing  
547 time. Each was converted to the same vertical reference system as GLISTIN (WGS84)  
548 using Vdatum then projected into the UTM coordinate system and resampled to 10 m  
549 using bilinear interpolation. The pixel resolution was resampled to 10 m so that it was  
550 standard across all regions. Before resampling, the pixel resolution of the NED differed  
551 by region, ranging from 8.5 m (northern Cascades, WA) to 9.4 m (Sierra Nevada, CA).  
552 GLISTIN was also resampled to 10 m and co-registered to the NED using the methods of

553 Berthier et al. (2007). The co-registration process reduces the horizontal and vertical  
554 offsets between the DEMs by first minimizing the standard deviation of differences over  
555 control zones and then applying that shift to the whole DEM. Offsets between DEMs can  
556 significantly influence estimates of elevation change, particularly on steep slopes  
557 (Berthier et al., 2007).

558

559

560

561

562

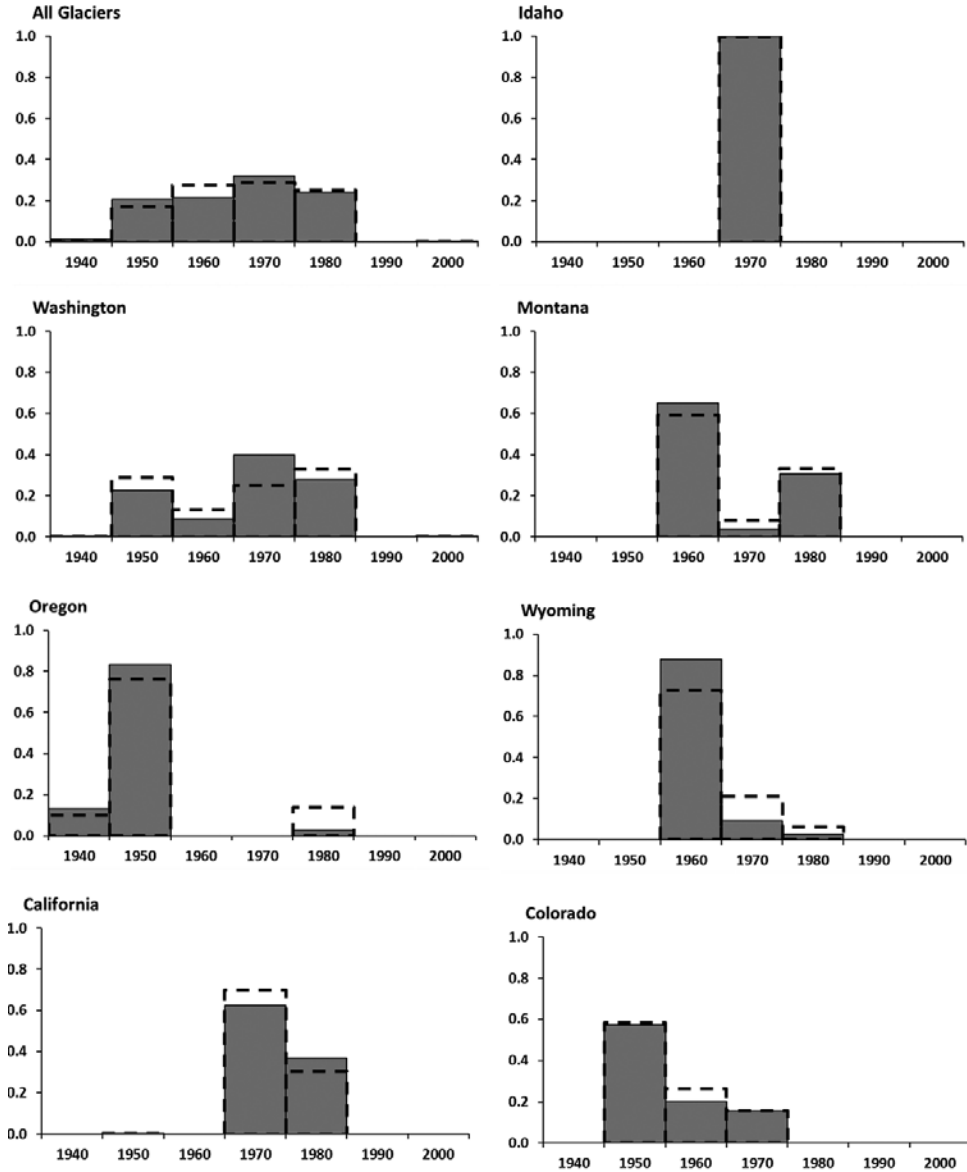
563

564

565

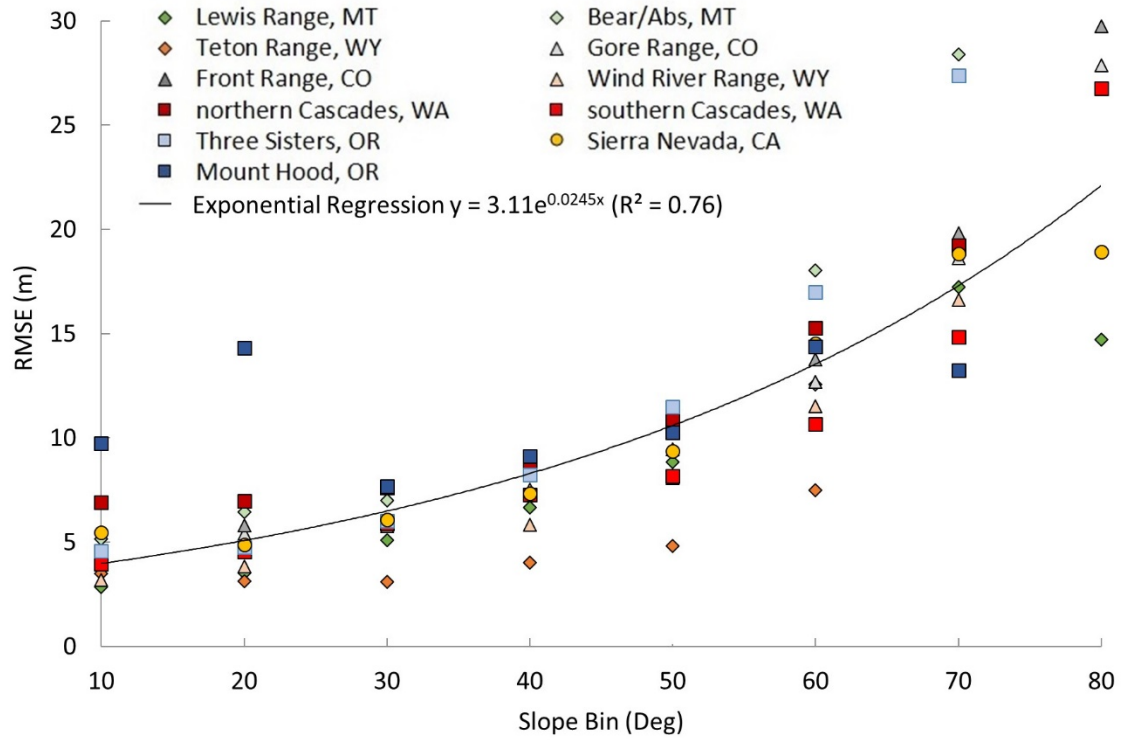
566

567



568  
 569 **Figure SOM1.** Acquisition dates for imagery used to create the U.S. Geological Survey  
 570 1:24000 topographic maps for areas with glaciers and perennial snowfields (G&PS). The  
 571 date on the x-axis represents the full decade (e.g., 1960 = 1960 to 1969). The y-axis is the  
 572 fraction of the total. The solid grey bars are the fraction of area, and the dashed outline is  
 573 the fraction of the number of G&PS. The top left depicts the imagery for all G&PS in the  
 574 western U.S. The other graphs show the acquisition date for each state. Reprinted from  
 575 Fountain et al. (2017).  
 576





578

579 **Figure SOM2.** Root mean square error (RMSE) between GLISTIN elevations and the  
 580 National Elevation Dataset for control zones binned by 10° slopes. The slope label  
 581 represents the maximum of that bin. The 10° slope bin includes slopes of 0°.

582

583

584

585

586

587

588

589

590

591

592

593 **Table SOM1.** List of sources compiled for the historical elevation data. The three  
 594 sources used were the National Map, maintained by the U.S. Geological Survey (USGS),  
 595 the Oregon office of the Bureau of Land Management (BLM), and the Geomorphological  
 596 Research Group at the University of Washington (UW).  
 597

State/Range	Source	Website
<b>California</b>		
Sierra Nevada	USGS	<a href="https://viewer.nationalmap.gov/basic">https://viewer.nationalmap.gov/basic</a>
<b>Colorado</b>		
Front	USGS	<a href="https://viewer.nationalmap.gov/basic">https://viewer.nationalmap.gov/basic</a>
Gore	USGS	<a href="https://viewer.nationalmap.gov/basic">https://viewer.nationalmap.gov/basic</a>
<b>Montana</b>		
Beartooth-Absaroka	USGS	<a href="https://viewer.nationalmap.gov/basic">https://viewer.nationalmap.gov/basic</a>
Lewis	USGS	<a href="https://viewer.nationalmap.gov/basic">https://viewer.nationalmap.gov/basic</a>
<b>Oregon</b>		
Cascade	BLM	<a href="http://earthexplorer.usgs.gov">http://earthexplorer.usgs.gov</a>
<b>Washington</b>		
northern Cascades	UW	<a href="http://gis.ess.washington.edu/data/">http://gis.ess.washington.edu/data/</a>
northern Cascades	USGS	<a href="https://viewer.nationalmap.gov/basic">https://viewer.nationalmap.gov/basic</a>
southern Cascades	BLM	<a href="http://earthexplorer.usgs.gov">http://earthexplorer.usgs.gov</a>
<b>Wyoming</b>		
Teton	USGS	<a href="https://viewer.nationalmap.gov/basic">https://viewer.nationalmap.gov/basic</a>
Wind River	USGS	<a href="https://viewer.nationalmap.gov/basic">https://viewer.nationalmap.gov/basic</a>

598  
 599  
 600  
 601  
  
 602  
  
 603  
  
 604  
  
 605  
  
 606  
 607

608 **Table SOM2.** List of lidar datasets used for the absolute error assessment. The datasets  
 609 came from three sources, the National Map, maintained by the U.S. Geological Survey  
 610 (USGS; <https://viewer.nationalmap.gov/basic/>), Washington Department of Natural  
 611 Resources (WA DNR; <https://lidarportal.dnr.wa.gov/>), and Oregon Department of  
 612 Geology and Mineral Industries (DOGAMI;  
 613 <https://gis.dogami.oregon.gov/maps/lidarviewer/>). ‘Uncertainty’ refers to the reported  
 614 absolute vertical uncertainty of the lidar.

<u>Region</u>	<u>Year</u>	<u>Source</u>	<u>Uncertainty</u>
Mount Adams, WA	2016	USGS	0.07
northern Cascade Range, WA	2009	WA DNR	0.04
Mount Rainier, WA	2007/2008	WA DNR	0.04
Three Sisters, OR	2010	DOGAMI	0.04

615  
 616  
 617  
 618  
 619

620 **Table SOM3.** Amount of missing data in GLISTIN mosaic based on the number of flight  
 621 passes. ‘Missing Area’ is the total area of pixels for the listed category in the GLISTIN  
 622 mosaic that had no elevation data. ‘Total Area’ is the total area of all pixels for the  
 623 category in the GLISTIN mosaic. ‘% Missing’ is the ratio of the missing area divided by  
 624 the total area within that category.

625

<u>Flight Passes</u>	<u>Missing Area (km<sup>2</sup>)</u>	<u>Total Area (km<sup>2</sup>)</u>	<u>% Missing</u>
1	8575.94	10259.58	83.59
2	5368.17	15877.95	33.81
3	1167.58	7344.92	15.90
4	912.02	6511.64	14.01
5	154.29	813.70	18.96
6	51.56	379.55	13.59
7	8.67	147.40	5.88
8	4.00	64.31	6.23

626  
 627  
 628  
 629  
 630

631 **Table SOM4.** Elevation uncertainty for control zones estimated from comparing  
632 GLISTIN, lidar, and National Elevation Dataset (NED). The sources and accuracy of the  
633 lidar data are listed in the supplementary online material. ‘Region’ refers to the region of  
634 the mosaicked GLISTIN digital elevation models, ‘Area’ is the area of the control zone,  
635 ‘Swath Count’ is a range of the number of GLISTIN flights covering the control zones,  
636 and standard deviation, ‘RMSE’ is the root mean square error. The ‘All’ column  
637 combines data from the three regions (columns to the left) with multiple GLISTIN  
638 passes.

	northern Cascades, WA	Mount Rainier, WA	Three Sisters, OR	All	Mount Adams, WA
Lidar Year	2009	2007/08	2010	---	2016
Area (km <sup>2</sup> )	1.61	3.10	1.95	6.66	12.74
Swath Count	3-6	3-4	2	2-6	1
<b>GLISTIN minus lidar</b>					
RMSE (m)	+1.79	+1.87	+1.64	+1.78	+3.20
Mean ± std (m)	-0.14 ± 1.78	+0.38 ± 1.83	+0.10 ± 1.63	+0.17 ± 1.78	0.00 ± 3.20
Median (m)	-0.08	+0.17	+0.15	+0.11	0.00
<b>GLISTIN minus NED</b>					
RMSE (m)	+8.84	+3.36	+7.14	+6.46	+6.22
Mean ± std (m)	+4.49 ± 7.61	+0.57 ± 3.31	-2.05 ± 6.84	+1.05 ± 6.38	+0.49 ± 6.20
Median (m)	+4.83	+035	-0.49	+0.80	+0.52
<b>Lidar minus NED</b>					
RMSE (m)	+7.21	+2.27	+8.37	+5.89	+5.60
Mean ± std (m)	+0.13 ± 7.21	-0.21 ± 2.27	-2.87 ± 7.86	-0.89 ± 5.83	-0.18 ± 5.60
Median (m)	+0.54	-0.15	-0.62	-0.19	-0.03

639  
640  
641  
642  
643  
644  
645  
646

647 **Table SOM5.** Root mean square error (RMSE), and mean elevation difference between  
 648 the National Elevation Dataset and GLISTIN derived elevations of barren earth control  
 649 zones, and total area (Area) of the barren earth control zones in each region sampled.

<b>Region</b>	<b>RMSE (m)</b>	<b>Mean ± std (m)</b>	<b>Area (km<sup>2</sup>)</b>
northern Cascades, WA	7.74	+0.33 ± 7.73	107.34
southern Cascades, WA	5.81	+0.62 ± 5.83	27.06
Mount Hood, OR	8.26	-2.42 ± 8.25	10.21
Three Sisters, OR	6.07	+0.64 ± 6.03	23.19
Sierra Nevada, CA	6.64	-1.72 ± 6.42	191.16
Lewis, MT	8.89	+1.72 ± 8.80	22.16
Beartooth-Absaroka, MT	10.57	-0.26 ± 10.57	7.83
Teton, WY	3.53	-0.32 ± 3.52	0.93
Wind River, WY	6.55	-0.96 ± 6.48	7.81
Front, CO	8.31	+1.40 ± 8.19	36.54
Gore, CO	8.15	+1.68 ± 7.98	27.43
<b>Total</b>	<b>7.32</b>	<b>-0.37 ± 7.31</b>	<b>461.67</b>

650  
 651  
 652  
 653  
 654  
 655  
 656  
 657  
 658  
 659  
 660  
 661  
 662  
 663  
 664

665 **Table SOM6.** Volume change estimates for glaciers and perennial snowfields in select  
666 regions and periods. Volume change was estimated between the initial NED year and the  
667 GLISTIN year of 2016 for glaciers and perennial snowfields with  $\geq 80\%$  GLISTIN. The  
668 change was grouped by region and year. The year listed is the last in the 5-year interval  
669 (e.g., 1955 = 1951 to 1955). ‘Num’ is the number of G&PS for that category.  
670

Region/Year/Type	Num	Area (km <sup>2</sup> )	Volume Change (m <sup>3</sup> x 10 <sup>6</sup> )	Specific Vol Change (m)	Specific Vol Change Rate (m yr <sup>-1</sup> )
<b>WA Cascades</b>					
1960	75	19.70	-336.81 ± 117.49	-17.10 ± 5.96	-0.31 ± 0.11
Glacier	29	17.75	-312.42 ± 106.56	-17.60 ± 6.00	-0.31 ± 0.11
Snowfield	46	1.95	-24.40 ± 10.93	-12.48 ± 5.59	-0.22 ± 0.10
1970	53	53.36	-507.94 ± 255.44	-9.52 ± 4.79	-0.21 ± 0.10
Glacier	23	52.40	-501.59 ± 250.65	-9.57 ± 4.78	-0.21 ± 0.10
Snowfield	30	0.96	-6.35 ± 4.79	-6.62 ± 5.00	-0.14 ± 0.11
1975	82	15.88	-290.34 ± 124.61	-18.29 ± 7.85	-0.45 ± 0.19
Glacier	24	13.14	-249.19 ± 102.35	-18.96 ± 7.79	-0.46 ± 0.19
Snowfield	58	2.73	-41.16 ± 22.26	-15.05 ± 8.14	-0.37 ± 0.20
1980	20	21.40	-320.08 ± 180.75	-14.95 ± 8.44	-0.42 ± 0.23
Glacier	8	20.81	-309.81 ± 175.82	-14.89 ± 8.45	-0.41 ± 0.23
Snowfield	12	0.59	-10.27 ± 4.94	-17.32 ± 8.33	-0.48 ± 0.23
1985	101	34.14	-662.12 ± 275.94	-19.39 ± 8.08	-0.63 ± 0.26
Glacier	40	31.54	-628.40 ± 257.10	-19.92 ± 8.15	-0.64 ± 0.26
Snowfield	61	2.60	-33.71 ± 18.83	-12.97 ± 7.25	-0.42 ± 0.23
<b>OR Cascades</b>					
1960	44	14.47	-215.07 ± 90.29	-14.86 ± 6.24	-0.27 ± 0.11
Glacier	13	12.19	-188.44 ± 76.15	-15.46 ± 6.25	-0.28 ± 0.11
Snowfield	31	2.28	-26.63 ± 14.14	-11.67 ± 6.19	-0.21 ± 0.11
1975	25	8.09	-143.32 ± 50.91	-17.71 ± 6.29	-0.43 ± 0.15
Glacier	9	7.44	-137.50 ± 46.93	-18.48 ± 6.31	-0.45 ± 0.15
Snowfield	16	0.65	-5.83 ± 3.98	-8.97 ± 6.13	-0.22 ± 0.15
<b>Sierra Nevada</b>					
1975	16	0.39	-4.19 ± 2.38	-10.74 ± 6.09	-0.26 ± 0.15
Glacier	2	0.13	-1.85 ± 0.73	-14.57 ± 5.73	-0.36 ± 0.14
Snowfield	14	0.26	-2.35 ± 1.65	-8.90 ± 6.26	-0.22 ± 0.15
1980	35	2.61	-42.98 ± 18.44	-16.44 ± 7.05	-0.46 ± 0.20
Glacier	12	1.95	-34.69 ± 13.74	-17.76 ± 7.04	-0.49 ± 0.20
Snowfield	23	0.66	-8.30 ± 4.70	-12.55 ± 7.10	-0.35 ± 0.20
1985	109	3.87	-40.62 ± 18.78	-10.50 ± 4.86	-0.34 ± 0.16
Glacier	9	1.40	-19.27 ± 8.63	-13.79 ± 6.18	-0.44 ± 0.20
Snowfield	100	2.47	-21.35 ± 10.15	-8.64 ± 4.11	-0.28 ± 0.13
<b>Wind River</b>					
1970	64	23.95	-365.80 ± 115.43	-15.28 ± 4.82	-0.33 ± 0.10
Glacier	19	21.17	-345.41 ± 102.55	-16.31 ± 4.84	-0.35 ± 0.11
Snowfield	45	2.77	-20.40 ± 12.89	-7.35 ± 4.64	-0.16 ± 0.10

1975	24	0.60	-3.61 ±	2.82	-6.01 ± 4.70	-0.15 ± 0.11
Glacier	1	0.05	-1.12 ±	0.27	-20.90 ± 4.96	-0.51 ± 0.12
Snowfield	23	0.55	-2.49 ±	2.56	-4.55 ± 4.68	-0.11 ± 0.11

671  
672  
673

1  
2                   **Application of Aerial InSAR to Measure Glacier Elevations**

3  
4 **Bryce Glenn<sup>1</sup>, Andrew G. Fountain<sup>1</sup>, Delwyn Moller<sup>2</sup>**

5  
6 <sup>1</sup> Department of Geology, Portland State University, Portland, Oregon, USA 97207

7 <sup>2</sup> Department of Electrical, Computer & Software Engineering, University of Auckland,  
8 Auckland, New Zealand

9  
10 Corresponding author: Andrew G. Fountain, [andrew@pdx.edu](mailto:andrew@pdx.edu)

11  
12  
13 **Key Points:**

- 14       • Aerial InSAR can rapidly map the topography of alpine glaciers over a broad  
15       region.
- 16       • Elevations compare favorably to lidar,  $+0.17 \pm 1.78$  m at spatial scale of 3 m.
- 17       • The mean rate of glacier elevation change (specific volume) is  $-0.3 \pm 0.2$  m yr<sup>-1</sup>  
18       for the past 56 years with rates increasing since 1980.

19  
20



21 **Abstract**

22

23 Glaciers and perennial snowfields are important to alpine ecosystems and regional  
24 hydrology. Quantifying volume change of a population of glaciers widely distributed  
25 over a region is difficult and expensive. We employed NASA's novel Airborne Glacier  
26 and Ice Surface Topography Interferometer (GLISTIN) to rapidly map surface  
27 topography of alpine glaciers across the western USA. In five flight days 3289 glaciers  
28 and perennial snowfields were surveyed. Comparison with lidar over control sites showed  
29 a mean difference of  $+0.17 \pm 1.78$  m at a spatial scale of 3 m. Data coverage increased  
30 and elevation uncertainty decreased with the mosaicking of multiple passes due to the  
31 complex terrain. Elevation change since the National Elevation Dataset shows a thinning  
32 (and volume loss) over the last ~56 years, averaging  $-0.3 \pm 0.2$  m and accelerating since  
33 1980. GLISTIN can be a valuable tool for rapidly mapping ice surfaces in the alpine  
34 environment.

35

36 **Plain Language Summary**

37

38 Glaciers and perennial snowfields are important water sources to alpine ecosystems and  
39 regional hydrology. To quantify their contribution their volume change is measured by  
40 mapping elevation changes of the ice surface. However, quantifying volume change for a  
41 population of glaciers widely distributed over a region is difficult and expensive. We  
42 employed NASA's airborne radar (GLISTIN) to rapidly map surface topography of  
43 alpine glaciers across the western USA. In only five flight days 3289 glaciers and  
44 perennial snowfields were surveyed. GLISTIN data over control-regions were compared  
45 to lidar, an independent elevation measure using lasers, and showed small differences  
46 indicating this method can be a valuable and cost-effective tool to track glacier change in  
47 the future. Comparing the new elevations against historic elevations from USGS maps a  
48 dramatic thinning (and volume loss) over the last ~60 years.

49

50 **1. Introduction**

51

52 Glacier melt is important to runoff in high alpine landscapes. At a local scale, melting  
53 glaciers maintain streamflow during the dry, late summer months after the seasonal snow

54 has melted (Fountain & Tangborn, 1985; Moore et al., 2009). Shrinking glaciers lose ice  
55 volume and supply more water to streams and rivers than anticipated from precipitation.  
56 Although this may be a temporary benefit, particularly in dry regions, their ability to  
57 buffer seasonal runoff in future is reduced, making watersheds more vulnerable to  
58 drought (Hall & Fagre, 2003; Moore et al., 2009). At a global scale, mass transfer of  
59 water from storage as ice to water runoff increases global sea-levels (Meier, 1984; Pfeffer  
60 et al., 2014; Zemp et al., 2019).

61

62 Traditionally, tracking glacier mass change was a field effort based on measuring the gain  
63 and loss of snow and ice at points on the glacier (Kaser et al., 2003; Ostrem & Brugman,  
64 1991). Although these efforts produce high-quality results showing spatial variations in  
65 mass change across a glacier only a few glaciers can be so monitored by any agency  
66 (Andreassen et al., 2005; O’Neel et al., 2019). Remote-sensing methods can be used to  
67 cover broad regions using an alternative approach that estimates mass change from  
68 volume change. Differential interferometric synthetic aperture radar (InSAR) can map  
69 surface elevation changes and offers the advantage of an all-weather, day/night  
70 capability, a particularly valuable tool in often cloudy alpine environments (Rosen et al.,  
71 2000). Satellite-borne applications have revolutionized our understanding of Antarctica  
72 and Greenland (Mouginot et al., 2019; Shepherd et al., 2018), and more recently, the  
73 larger alpine glaciers (Millan et al., 2022). Challenges using InSAR include shadowing,  
74 decorrelation due to layover, phase unwrapping, and temporal landscape changes  
75 (Eineder & Holzner, 2000; Rees, 2000).

76

77 Here, we test a novel approach for determining surface elevations on alpine glaciers using  
78 an airborne single-pass InSAR, NASA’s Glacier, and Ice Surface Topography  
79 Interferometer (GLISTIN; Moller et al., 2017). Unlike differential/repeat-pass InSAR,  
80 GLISTIN collects two radar images simultaneously, allowing elevations to be derived  
81 from a single flight pass and are thus not sensitive to temporal decorrelation between  
82 observations. Mounted on a jet aircraft, GLISTIN can image large areas in a short time  
83 and has been used to map the relatively gentle topography of large glaciers and ice sheets

84 (Hensley et al., 2016; Moller et al., 2019). We evaluate its performance to map small  
85 alpine glaciers in complex terrain across a broad region. In addition, the updated glacier  
86 elevations are differenced from the National Elevation Data (Gesch, 2002) to calculate  
87 glacier elevation change across the western US.

88

## 89 **2. Data and Methods**

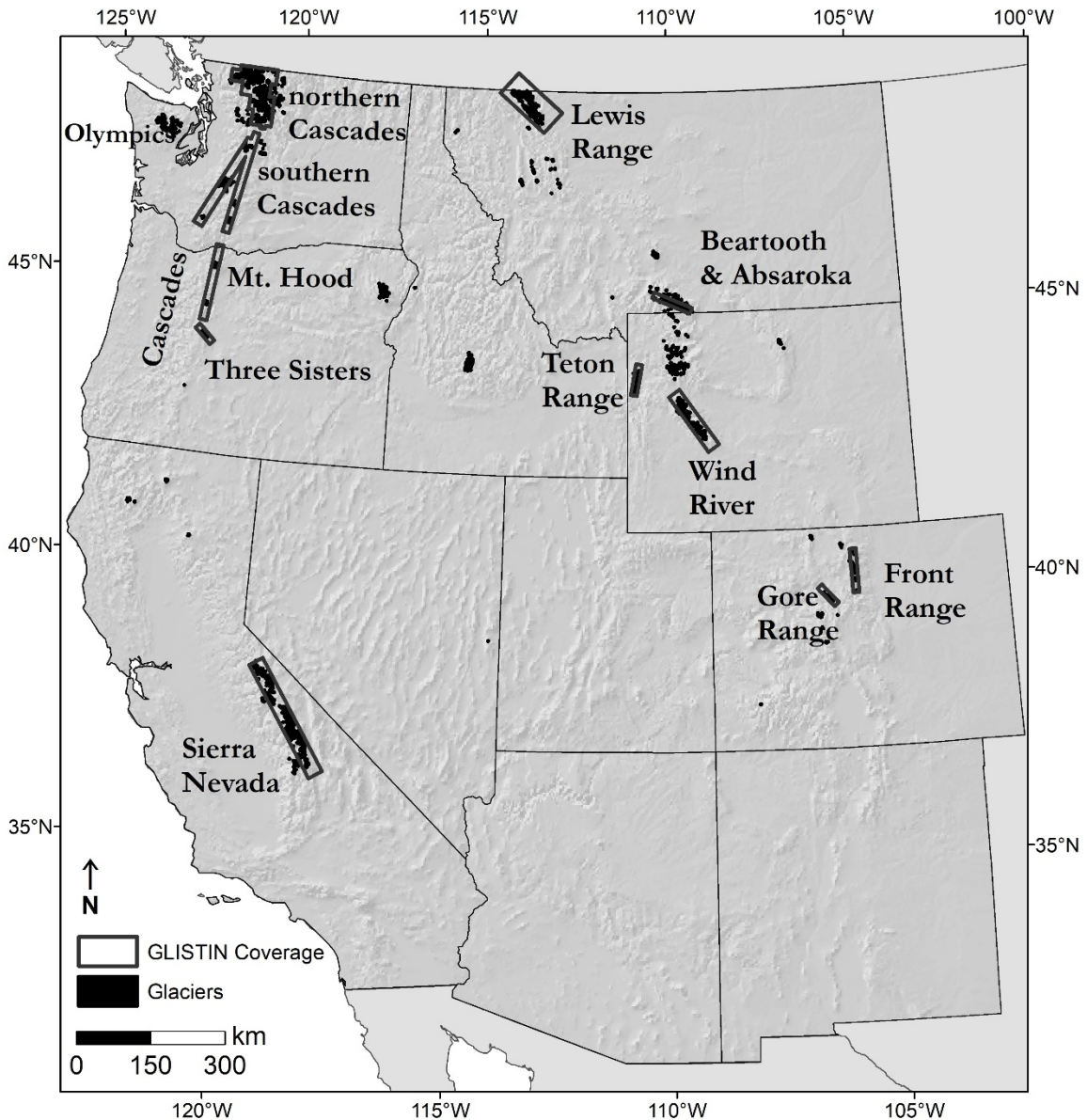
90

### 91 2.1 Study Area

92

93 The study region is the American West, defined as the continental United States west of  
94 the 100th meridian enclosing about  $2 \times 10^6$  km<sup>2</sup> and home to about 5036 glaciers and  
95 perennial snowfields ( $\geq 0.01$  km<sup>2</sup>) as of the late 20<sup>th</sup> century (Figure 1; Fountain et al.,  
96 2017). The region is made up of three large mountain ranges, the Rocky Mountains, the  
97 Cascade Range, and the Sierra Nevada. Many peaks exceed 4000 m in. The largest  
98 concentration of glaciers, and lowest elevation (2000 m - 3000 m asl) is in the maritime  
99 climate of the Pacific Northwest (Oregon, Washington, north-west Montana,). The  
100 remaining glaciers are in continental climates elsewhere at high elevations, > 3000m.

101



102  
 103 **Figure 1.** Map of glaciers and perennial snowfields (black dots) in the Western U.S. The  
 104 boxes show regions surveyed by GLISTIN.

105  
 106 Regional studies have shown drastic decreases in glacier area exceeding 50% over the  
 107 last century (DeVisser & Fountain, 2015; Fagre et al., 2017; O’Neal et al., 2019). The  
 108 rate of change has not been constant or spatially uniform (Basagic & Fountain, 2011;  
 109 Hoffman et al., 2007; O’Neal et al., 2015). Glacier volume changes, estimated by  
 110 differencing topography over time, show a loss on Mount Rainier, WA, of  $-0.65 \text{ km}^3$ ,

111 average specific mass loss rate of  $-0.16 \text{ m w.e yr}^{-1}$  (1970 - 2007/2008; Sisson et al.,  
112 2011). Menounos et al. (2018) estimated a volume loss of  $-127.65 \pm 45.17 \text{ km}^3$ ,  $-0.42 \pm$   
113  $0.15 \text{ m w.e.}$  between 2000 and 2018 for most of the glaciated terrain in Western North  
114 America.

## 115 116 2.2 GLISTIN

117  
118 GLISTIN is a Ka-band radar (8.4 mm, 35.66 GHz) system that utilizes two horizontally  
119 polarized antennas, 0.25 m apart in elevation, both of which are capable of transmitting  
120 and receiving (Moller et al., 2019). Unlike repeat-pass InSAR, GLISTIN's dual antennas,  
121 collect data simultaneously. The Ka-band center frequency enables high accuracy with a  
122 compact architecture and reduces snow penetration compared to lower frequencies. This  
123 cross-track InSAR system is capable of providing not only the position of each image  
124 point in along-track and slant range as with traditional SAR but also the height of that  
125 point via the interferometric phase. Because the phase repeats after  $2\pi$ , it must be  
126 "unwrapped" to determine its unique location and height relative to a reference surface  
127 (Moller et al., 2011; Rosen et al., 2000). The system is contained in an external pod  
128 beneath NASA's Gulfstream-III aircraft with left looking view angles of  $15\text{-}50^\circ$  from  
129 nadir. The system is coupled to inertial navigation and global position that provide pitch  
130 and roll of the aircraft as well as its precise position in space. Nominal flight altitudes are  
131 about 12,500 m above sea-level with a ground swath width of about 12 km and its typical  
132 air speed is  $720 \text{ km hr}^{-1}$ .

133  
134 To guide the aerial survey, the locations of the glaciers were retrieved from Fountain et  
135 al. (2017). Flight passes were typically flown in pairs, each in an opposite direction, to  
136 reduce gaps in backscatter from radar shadow or layover in the mountainous terrain. In a  
137 few regions additional perpendicular flight passes were also flown. The georectified  
138 height-maps from each pass were mosaicked into a 3-meter pixel-size digital elevation  
139 model (DEM; Hensley et al., 2016) and projected into the Universal Transverse Mercator  
140 (UTM) coordinate system. Self-reported elevation accuracy is 'height-precision', a  
141 statistical estimate based on the interferometric correlation of each individual radar pixel

142 making up the 3 m mosaicked pixel (Moller et al., 2011). In the final mosaicked DEM,  
143 the elevation of each pixel is the weighted sum of elevations from individual passes and  
144 the weights are inversely proportional to the height-precision (Hensley et al., 2016). The  
145 vertical absolute uncertainty of GLISTIN-derived topography was found to be about  $\pm$   
146 0.30 m over bare non-snow-covered terrain (Schumann et al., 2016). Data collection and  
147 processing were provided by the Jet Propulsion Laboratory at California Institute of  
148 Technology, Pasadena, CA.

### 149 150 2.3 Accuracy

151  
152 The accuracy of GLISTIN elevations was ground-truthed by differencing lidar DEMs  
153 from GLISTIN DEMs (Table SOM2). All lidar data were converted from its native  
154 coordinate system to WGS84 to UTM using Vdatum (Version 3.8, 2017, National  
155 Oceanic and Atmospheric Administration, Washington, DC), inducing an error of about  
156 0.076 m (self-reported by Vdatum during conversion) and resampled to 3 m to match the  
157 GLISTIN DEMs spatial posting, using bilinear interpolation. To calculate elevation  
158 change the  $\frac{1}{3}$  arc-second NED was converted to UTM (WGS84) using Vdatum and  
159 resampled to 10 m using bilinear interpolation. GLISTIN and lidar elevations were also  
160 resampled to 10 m using bilinear interpolation to match the NED. The relative accuracy  
161 of GLISTIN, lidar, and the NED were inter-compared at four barren earth snow-free  
162 control zones in the Cascade Range of Oregon and Washington where all three estimates  
163 of elevation were available. Each control zone is a patchwork of co-located but isolated  
164 terrains. Barren earth terrains were derived from the 'barren' class of the 2016 National  
165 Land Cover Database (<https://www.mrlc.gov/data/nlcd-2016-land-cover-conus>).  
166 GLISTIN's performance imaging ice/snow surfaces was examined by comparing  
167 elevations to lidar data acquired on Mount Adams, Washington, which was flown 28  
168 days prior to the GLISTIN flights. We expect GLISTIN to yield somewhat lower  
169 elevations due to melting of the snow and ice.

170  
171  
172

173 2.4 Area and Volume Change

174

175 The reference area and elevation of the glaciers and perennial snowfields are derived  
176 from (Fountain et al., 2017) and a ‘historic’ version of the NED (Gesch et al., 2002),  
177 respectively. Both are based on the original U.S. Geological Survey 1:24000 topographic  
178 maps from which the glacier outlines and elevations were derived. The maps in the  
179 western US were drawn over a period of years (1940s-1980s. Resolution of the NED is  $\frac{1}{3}$   
180 arc-second ( $\sim 10$  m), and the horizontal and vertical coordinate systems are North  
181 American Datum of 1983, North American Vertical Datum of 1988, respectively. The  
182 NED is continually being updated and it was necessary to retrieve the original ‘historic’  
183 version from multiple sources (Table SOM1).

184

185 Volume change was estimated by differencing the GLISTIN elevations from the NED  
186 elevations within the original perimeter and for only those glaciers with  $\geq 80\%$  GLISTIN  
187 coverage. Le Bris and Paul (2015) showed that good estimates of volume change can be  
188 achieved with the elevation postings cover at least 80% of the glacier area. Reasonable  
189 estimates of volume change can be obtained for coverages as low as 40%, however  
190 results depend on interpolation method (McNabb et al., 2019), so we adopted the more  
191 conservative threshold of 80% used by Le Bris and Paul (2015). In order to compare  
192 volume loss between large and small glaciers and because the historic mapping occurred  
193 over a time-span of decades across the western US, results are expressed as the rate of  
194 specific volume (volume/area) change ( $\text{m}^{-3} \text{m}^{-2} \text{yr}^{-1}$  or  $\text{m} \text{yr}^{-1}$ ).

195

196 Uncertainty of volume change,  $\sigma_{\Delta V}$ , is calculated for each individual glacier or perennial  
197 snowfield, using the vertical and area uncertainties (Menounos et al., 2018),

198 
$$\sigma_{\Delta V} = \sqrt{(\sigma_{\Delta z} A_g)^2 + (\sigma_A \Delta z)^2}, \quad (1)$$

199

200 where  $\sigma_{\Delta z}$  is the RMSE of elevation differences between GLISTIN and the NED for all  
201 barren earth control zones, for the region in which the glacier or perennial snowfield is  
202 located,  $A_g$  is the original (historic) area of the glacier or perennial snowfield,  $\Delta z$  is the

203 average elevation change of the glacier or perennial snowfield, and  $\sigma_A$  is area uncertainty.  
204 Uncertainty of the original areas is considered 9% (Fountain et al., 2017).

205

### 206 3. Results and Analysis

207

#### 208 3.1 Data collection

209

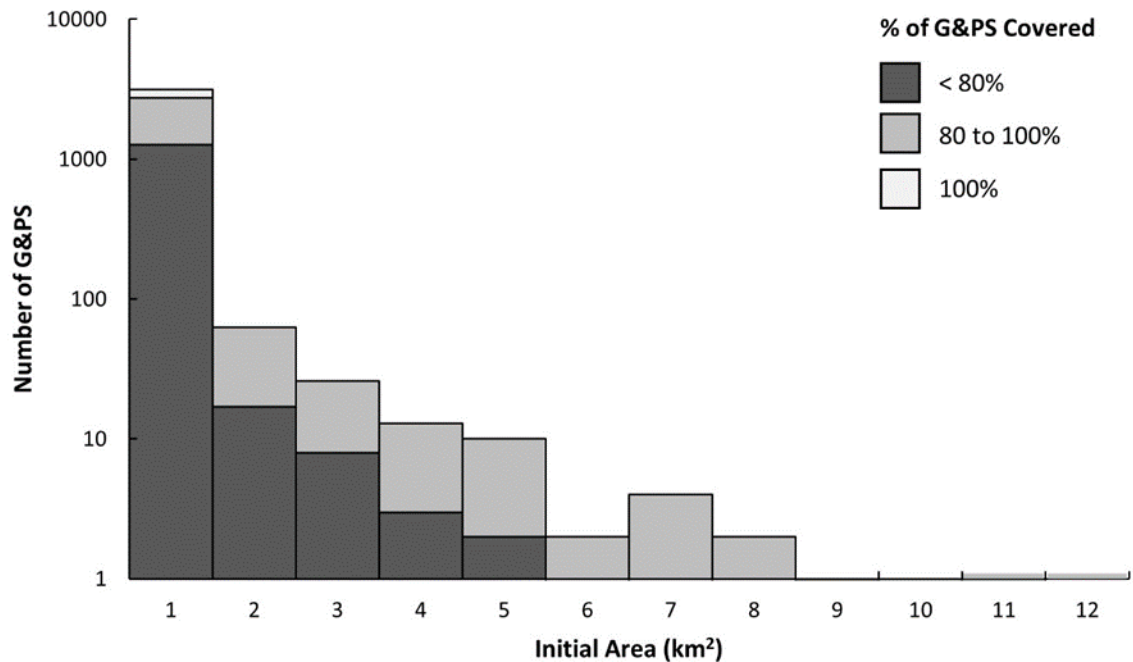
210 The GLISTIN flights imaged the glacier-populated mountains of the American West for  
211 5 flight days, between September 12 to 28, 2016, covering about 41,000 km<sup>2</sup> (Figure 1).

212 Due to an unexpected reassignment of the aircraft, several mountain ranges were not  
213 included, most notably the Olympic Mountains, WA, and the Absaroka Range, WY.

214 Within the regions surveyed 3889 glaciers and perennial snowfields are present.

215 GLISTIN coverage of each varied from 0 to 100% with a median of 81%. The total  
216 number of features with  $\geq 80\%$  coverage was 1770 (309 km<sup>2</sup>, 53% of the total area of  
217 surveyed G&PS; figure 2).

218



219

220 **Figure 2.** Histogram of the initial area of glaciers and perennial snowfields and the

221 fraction of area mapped by GLISTIN. Initial area refers to the area from the U.S.

222 Geological Survey's 1:24000 map series. The x-axis value is the maximum for each bin.



223

224

225 As expected, increasing the number of flight passes over the same area increased the  
226 backscatter coverage. For one flight pass backscatter was received from 17% of the entire  
227 illuminated area, for two flights 66%, four flights, 86%, and for eight flights 94% (Table  
228 SOM3). No significant difference was observed in backscatter coverage of snow/ice  
229 surfaces compared to ice-free surfaces, and within glaciers no significant differences  
230 between snow-covered regions and ice-exposed regions. Backscatter reception was only  
231 significantly correlated with terrain slope with greater loss on steeper slopes.

232

### 233 3.2 Accuracy

234

235 The GLISTIN DEMs for three of the four barren earth control zones were compiled from  
236 multiple passes. The fourth control zone (Mount Adams, WA) was comprised of single  
237 pass data and was examined separately. For the three multi-pass barren earth control  
238 zones the GLISTIN – lidar (3 m posting) mean difference was  $+0.17 \pm 1.78$  m (Table  
239 SOM4). Comparing GLISTIN and the NED over the same regions (10 m posting), the  
240 mean difference and standard deviation was much larger,  $+1.05 \pm 6.38$  m. This is due to  
241 the much larger uncertainty in the NED elevations of 3.74 m, which is based mostly on  
242 control points located in lower elevation and less complex terrain (Gesch, 2007). The  
243 mean lidar-NED difference  $-0.89 \pm 5.83$ , supports this inference. For the control zones on  
244 Mount Adams, the mean elevations difference of single-pass GLISTIN - lidar (3 m  
245 posting) was  $-0.00 \pm 3.20$  m, whereas for the snow/ice surfaces it was  $-0.86 \pm 3.76$  m.  
246 The negative difference for the snow/ice surfaces is to be expected given the melting that  
247 occurred over the 28-day period between the initial lidar survey followed by the  
248 GLISTIN survey. Given that the snow is wet during this time of year and interferometric  
249 penetration is negligible (Hensley et al., 2016).

250 With respect to interferometric radar errors it is important to note that the height precision  
251 is dominated by the instrument random noise. This relative error is high frequency and  
252 will scale with spatial averaging of uncorrelated pixels or independent samples. The  
253 same is not true for the height accuracy or systematic (mean) offset which does not

254 improve with averaging as they are correlated. Therefore, if we calculate the RMSE for  
255 more coarse spatial postings this metric will reduce significantly (with the random  
256 /precision inversely proportional to the square-root of the effective number of  
257 independent looks (Hensley et. al. 2016). For this paper we analyze GLISTIN data at a  
258 spatial posting of 3m due to the small footprint of many of these glaciers. However, one  
259 can expect significantly improved height precision, and thereby RMSE for large glaciers  
260 via spatial averaging. The low mean difference (i.e. accuracy) observed for the barren  
261 areas indicates that extremely low height errors are achievable with sufficient spatial  
262 averaging to reduce the random component (Schumann et. al. 2016; Moller et.al. 2019)

263 Although no correlation was observed between mean elevation difference (GLISTIN -  
264 lidar) and surface slope, the standard deviation increased from about 1.7 m for slopes  
265 between 20° and 30° to 3.8 m for slopes between 50° and 60°. The RMSE (GLISTIN-  
266 NED) increased from 6.1 m for slopes 20° to 30° to 10.2 m for slopes between 50° and  
267 60°. The rate of phase change is a function of the interferometric measurement geometry  
268 and is directly proportional to the local slope. Phase unwrapping becomes more difficult  
269 as the slope increases so an increased RMSE in extreme topography is to be expected.  
270 The orientation of single-pass GLISTIN relative to the terrain surface affects the  
271 elevation difference. The mean elevation difference (GLISTIN-lidar) was smaller for  
272 surfaces facing towards GLISTIN,  $+0.01 \pm 2.07$  m, than surfaces facing away,  $+0.07 \pm$   
273  $4.03$  m.

### 274 3.3 Volume change

275  
276 Volume change was estimated for 1770 glaciers and perennial snowfields (54% of total)  
277 consisting of 351 glaciers and 1419 snowfields. Overall mean uncertainty, based on  
278 barren earth control zones across the west (Table SOM5), was  $-0.37 \pm 7.31$  m. Rejecting  
279 those specific volume changes that were smaller than uncertainty yielded 231 glaciers  
280 totaling  $198.84 \text{ km}^2$  and 551 perennial snowfields ( $21.31 \text{ km}^2$ ). Comparing our volume  
281 change to a prior estimate for Mt. Rainier, Washington (Sisson et al., 2011), showed that  
282 the prior estimate, based on a lidar-NED difference, of  $-8.6$  m (1970-2007) is within the

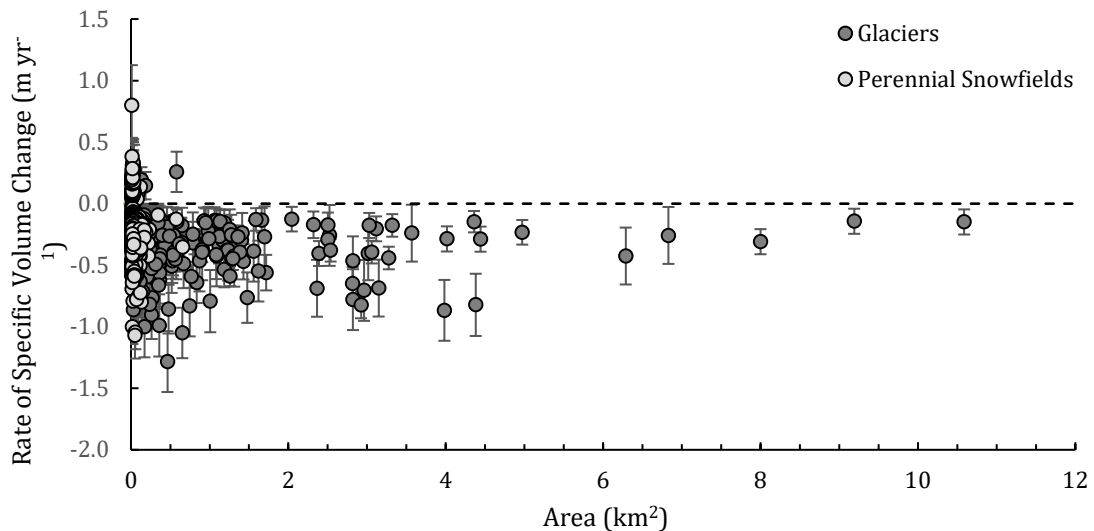
283 uncertainty of our value ,  $-9.7 \pm 4.8$  m (1970-2016). That our estimate showed a greater  
284 mass loss is consistent with the longer time period of comparison.

285

286 Most glaciers and perennial snowfields lost mass (Figure 3). The median rate of change  
287 for glaciers,  $-0.3 \pm 0.2$  m yr<sup>-1</sup>, and for snowfields,  $-0.2 \pm 0.2$  m yr<sup>-1</sup>. Four glaciers (2%)  
288 and 56 (10%) perennial snowfields increased in volume; their locations are not region  
289 specific. These features are characterized by small area, median 0.02 km<sup>2</sup> (all but one <  
290 0.2 km<sup>2</sup>), steeper slopes, and higher elevations. The features that gained volume were at  
291 significantly higher elevations and steeper slopes (median 3100 m, 28°) compared to  
292 those that lost volume, (median 2335 m 25°;  $p < 0.05$ , Mann-Whitney U). The time series  
293 of ice mass loss in the Cascade Range, Washington is relatively complete compared to  
294 other regions and show increasing mass loss with time (Figure 4). The rate of change  
295 increased significantly since 1980.

296

297



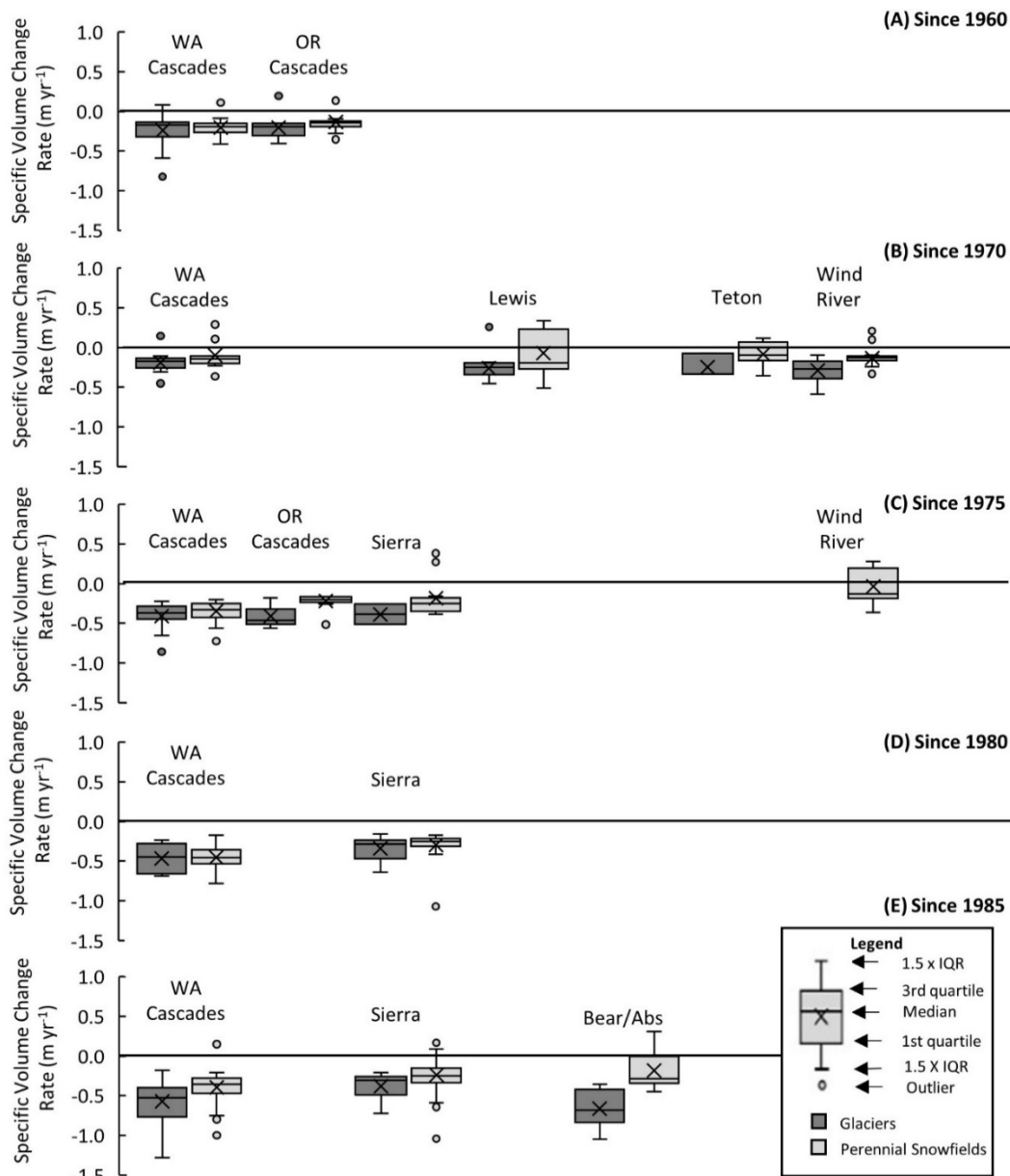
298

299 **Figure 3.** Specific volume change of glaciers and perennial snowfields (G&PS). Light  
300 grey circles represent perennial snowfields, and dark grey circles represent glaciers. The  
301 ‘whiskers’ represent uncertainty. Initial area refers to the area from the U.S. Geological  
302 Survey’s 1:24000 map series.

303

304

305  
306



307  
308

309 **Figure 4.** Volume change glaciers (dark grey boxes) and perennial snowfields (light grey  
310 boxes) for each region with more than ten features, grouped by initial mapping date (all  
311 ending in 2016), 1960 (1956 to 1960) (A), 1970 (1966 to 1970) (B), 1975 (1971 to 1975)  
312 (C), 1980 (1976 to 1980) (D), and 1985 (1981 to 1985) (E). The ‘whiskers’ represent the  
313 smallest and largest values not considered outliers. The values that exceed 1.5 times the  
314 interquartile range (IQR) below the first quartile or above the third quartile are  
315 considered outliers (open circles ‘Bear/Abs’ refers to Beartooth-Absaroka, MT).

316

#### 317 **4. Discussion and Conclusions**

318

319 GLISTIN was developed for measuring the relatively flat surfaces of large glaciers and  
320 ice sheets, and its application to the complex topography alpine terrain presents a stress-  
321 case for the instrument. GLISTIN elevation mosaics compared favorably to lidar  
322 measurements over barren earth  $+0.17 \pm 1.78$  m (3 m posting). Similar comparisons over  
323 bedrock in Greenland showed,  $+0.32 \pm 0.95$  m (30 m posting) for single pass elevations  
324 (Moller et al., 2019). Over snow and ice surfaces on Mount Adams the mean difference  
325 of GLISTIN and lidar was  $-0.87 \pm 3.8$  m (3 m posting). We regard much of the difference  
326 due to snow and ice melt over the 28-day interval between the initial lidar and later  
327 GLISTIN surveys. Similar mean GLISTIN – lidar differences, were observed on two  
328 gently sloping glacier surfaces in Alaska,  $+0.8 \pm 1.7$  m and  $+1.2 \pm 3.7$  m (3 m posting,  
329 Moller et al., 2019). There was a similarly substantial time interval between the GLISTIN  
330 and subsequent lidar surveys of 1.5 month and 1 month, respectively. Differencing  
331 GLISTIN from the NED for estimating historic glacier change showed the RMSE at  
332 control zones to be 7.35 m and largely driven by uncertainty in the NED.

333

334 The standard deviations for all elevation comparisons increased with surface slope and  
335 most likely due to small offsets in aligning the DEMs. This result is also common to  
336 other studies using matching DEMs. The mean elevation difference (Shuttle Radar  
337 Topography Mission 1 Arc-Second Global DEM) over non-glaciated terrain near the  
338 Akshirak glaciers (Tien Shan, Central Asia) was  $-4.5 \pm 10.9$  m for slopes between  $25^\circ$   
339 and  $30^\circ$ , increasing to  $-7.6 \pm 25.6$  m for slopes between  $40^\circ$  and  $78^\circ$  (Paul, 2008;  
340 Surazakov & Aizen, 2006). For North & Middle Sisters, Oregon the RMSE (lidar-NED)  
341 was 5.7 m and 12.3 m for slopes between  $20^\circ$  to  $30^\circ$  and  $50^\circ$  to  $60^\circ$ , respectively  
342 (Ohlschlager, 2015), and similar to the GLISTIN-NED RMSE of 6.4 m and 10.2 m for  
343 the same slope bins.

344

345 Elevations were acquired for 85% of the surveyed glaciers and perennial snowfields, of  
346 which 12% were completely mapped and 60% had  $\geq 80\%$  coverage. Increased number of

347 flight passes increased data coverage. This is one clear advantage over satellite InSAR  
348 that look direction can be easily changed. Most of the missing backscatter was caused by  
349 radar shadow and some from layover due to the steep terrain.

350

351 Rates of glacier specific mass loss across the western US are consistent with rates  
352 estimated by other studies in our region. Overall, our rates over the last period of our  
353 study 1985 - 2016 are consistent with the western US average (2000-2020) of about  $-0.4$   
354  $\text{m yr}^{-1}$  (Hugonnet et al., 2021). For the Cascade Range in Washington, Menounos et al.  
355 (2018) estimated  $-0.29 \pm 0.10 \text{ m yr}^{-1}$  (2000-2018) from DEMs derived from optical  
356 satellite imagery, which is half of our estimate of  $-0.63 \pm 0.26 \text{ m yr}^{-1}$  over the longer time  
357 period of 1985-2016. Furthermore, our historic (pre-2000) rates of change is similar to  
358 rates elsewhere globally (Andreassen et al., 2020; Carturan et al., 2013; DeBEER &  
359 Sharp, 2007; Lambrecht & Kuhn, 2007). We also note an acceleration in mass loss since  
360 1980.

361

362 GLISTIN makes an important contribution in tracking glacier change because data can be  
363 rapidly collected unimpeded by weather providing a near instantaneous elevation survey  
364 of glaciers across broad regions. It performed well in complex terrain exceeding its  
365 design requirement and future improvements in flight planning will reduce the  
366 uncertainty. Significantly improved uncertainty for larger glaciers is expected due to  
367 spatial averaging that reduces the random error component.

368

### 369 **Acknowledgments**

370 This work was supported by NASA grant NNX17AI59G. The authors would like to  
371 thank Yang Zhen and the GLISTIN group at JPL for their help in data processing and  
372 interpretation.

### 373 **Data Availability Statement**

374 Analyzed data are included as Supporting Information S1. The single radar swaths of  
375 elevation can be obtained from NASA, <https://uavsar.jpl.nasa.gov/cgi-bin/data.pl>, select

376 TopSAR (Ka-band). The mosaicked radar swaths used in this study can be found at,  
377 [https://pdxscholar.library.pdx.edu/geology\\_data/5/](https://pdxscholar.library.pdx.edu/geology_data/5/). The reference glacier outlines and  
378 elevations derived from the historic 1:24,000 USGS topographic maps and historic  
379 National Elevation Dataset (NED), respectively are located at,  
380 [https://pdxscholar.library.pdx.edu/geology\\_data/4/](https://pdxscholar.library.pdx.edu/geology_data/4/).

381

## 382 **References**

- 383 Andreassen, L. M., Elvehøy, H., Kjøllmoen, B., & Belart, J. M. C. (2020). Glacier  
384 change in Norway since the 1960s – an overview of mass balance, area, length  
385 and surface elevation changes. *Journal of Glaciology*, *66*(256), 313–328.  
386 <https://doi.org/10.1017/jog.2020.10>
- 387 Andreassen, L. M., Elvehøy, H., Kjøllmoen, B., Engeset, R. V., & Haakensen, N. (2005).  
388 Glacier mass-balance and length variation in Norway. *Annals of Glaciology*, *42*,  
389 317–325. <https://doi.org/10.3189/172756405781812826>
- 390 Basagic, H. J., & Fountain, A. G. (2011). Quantifying 20th Century Glacier Change in  
391 the Sierra Nevada, California. *Arctic, Antarctic, and Alpine Research*, *43*(3), 317–  
392 330. <https://doi.org/10.1657/1938-4246-43.3.317>
- 393 Carturan, L., Filippi, R., Seppi, R., Gabrielli, P., Notarnicola, C., Bertoldi, L., Paul, F.,  
394 Rastner, P., Cazorzi, F., Dinale, R., & Dalla Fontana, G. (2013). Area and volume  
395 loss of the glaciers in the Ortles-Cevedale group (Eastern Italian Alps): Controls  
396 and imbalance of the remaining glaciers. *The Cryosphere*, *7*(5), 1339–1359.  
397 <https://doi.org/10.5194/tc-7-1339-2013>
- 398 DeBEER, C. M., & Sharp, M. J. (2007). Recent changes in glacier area and volume  
399 within the southern Canadian Cordillera. *Annals of Glaciology*, *46*(1), 215–221.  
400 <https://doi.org/10.3189/172756407782871710>
- 401 DeVisser, M. H., & Fountain, A. G. (2015). A century of glacier change in the Wind  
402 River Range, WY. *Geomorphology*, *232*, 103–116.  
403 <https://doi.org/10.1016/j.geomorph.2014.10.017>

404 Eineder, M., & Holzner, J. (2000). Interferometric DEMs in alpine terrain-limits and  
405 options for ERS and SRTM. *IGARSS 2000. IEEE 2000 International Geoscience  
406 and Remote Sensing Symposium. Taking the Pulse of the Planet: The Role of  
407 Remote Sensing in Managing the Environment. Proceedings (Cat.  
408 No.00CH37120)*, 7, 3210–3212 vol.7.  
409 <https://doi.org/10.1109/IGARSS.2000.860385>

410 Fagre, D. B., McKeon, L. A., Dick, K. A., & Fountain, A. G. (2017). *Glacier margin time  
411 series (1966, 1998, 2005, 2015) of the named glaciers of Glacier National Park,  
412 MT, USA* [Data set]. U.S. Geological Survey. <https://doi.org/10.5066/f7p26wb1>

413 Fountain, A. G., Glenn, B., & Basagic, H. J. (2017). The Geography of Glaciers and  
414 Perennial Snowfields in the American West. *Arctic, Antarctic, and Alpine  
415 Research*, 49(3), 391–410. <https://doi.org/10.1657/AAAR0017-003>

416 Fountain, A. G., & Tangborn, W. V. (1985). The effect of glaciers on streamflow  
417 variations. *Water Resources Research*, 21(4), 579–586.

418 Gesch, D., Oimoen, M., Greenlee, S., Nelson, C., Steuck, M., & Tyler, D. (2002). The  
419 national elevation dataset. *Photogrammetric Engineering and Remote Sensing*,  
420 68(1), 5–32.

421 Hall, M. H., & Fagre, D. B. (2003). Modeled climate-induced glacier change in Glacier  
422 National Park, 1850–2100. *BioScience*, 53(2), 131–140.

423 Hensley, S., Moller, D., Oveisgharan, S., Michel, T., & Wu, X. (2016). Ka-Band  
424 Mapping and Measurements of Interferometric Penetration of the Greenland Ice  
425 Sheets by the GLISTIN Radar. *IEEE Journal of Selected Topics in Applied Earth  
426 Observations and Remote Sensing*, 9(6), 2436–2450.  
427 <https://doi.org/10.1109/JSTARS.2016.2560626>

428 Hoffman, M. J., Fountain, A. G., & Achuff, J. M. (2007). 20th-century variations in area  
429 of cirque glaciers and glacierets, Rocky Mountain National Park, Rocky  
430 Mountains, Colorado, USA. *Annals of Glaciology*, 46(1), 349–354.  
431 <https://doi.org/10.3189/172756407782871233>

432 Hugonnet, R., McNabb, R., Berthier, E., Menounos, B., Nuth, C., Girod, L., Farinotti, D.,  
433 Huss, M., Dussaillant, I., Brun, F., & Käab, A. (2021). Accelerated global glacier



434 mass loss in the early twenty-first century. *Nature*, 592(7856), 726–731.  
435 <https://doi.org/10.1038/s41586-021-03436-z>

436 Kaser, G., Fountain, A. G., & Jansson, P. (2003). *A manual for monitoring the mass*  
437 *balance of mountain glaciers* (No. 59; IHP-VI Technical Documents in  
438 Hydrology, p. 137). UNESCO.

439 Lambrecht, A., & Kuhn, M. (2007). Glacier changes in the Austrian Alps during the last  
440 three decades, derived from the new Austrian glacier inventory. *Annals of*  
441 *Glaciology*, 46(1), 177–184.

442 Le Bris, R., & Paul, F. (2015). Glacier-specific elevation changes in parts of western  
443 Alaska. *Annals of Glaciology*, 56(70), 184–192.  
444 <https://doi.org/10.3189/2015AoG70A227>

445 McNabb, R., Nuth, C., Kääh, A., & Girod, L. (2019). Sensitivity of glacier volume  
446 change estimation to DEM void interpolation. *The Cryosphere*, 13(3), 895–910.  
447 <https://doi.org/10.5194/tc-13-895-2019>

448 Meier, M. F. (1984). Contribution of small glaciers to global sea level. *Science*,  
449 226(4681), 1418–1421.

450 Menounos, B., Hugonnet, R., Shean, D., Gardner, A., Howat, I., Berthier, E., Pelto, B.,  
451 Tennant, C., Shea, J., Noh, M., Brun, F., & Dehecq, A. (2018). Heterogeneous  
452 changes in western North American glaciers linked to decadal variability in zonal  
453 wind strength. *Geophysical Research Letters*.  
454 <https://doi.org/10.1029/2018GL080942>

455 Millan, R., Mouginot, J., Rabatel, A., & Morlighem, M. (2022). Ice velocity and  
456 thickness of the world's glaciers. *Nature Geoscience*, 15(2), 124–129.  
457 <https://doi.org/10.1038/s41561-021-00885-z>

458 Moller, D., Andreadis, K. M., Bormann, K. J., Hensley, S., & Painter, T. H. (2017).  
459 Mapping Snow Depth From Ka-Band Interferometry: Proof of Concept and  
460 Comparison With Scanning Lidar Retrievals. *IEEE Geoscience and Remote*  
461 *Sensing Letters*, 14(6), 886–890.

462 Moller, D., Hensley, S., Mouginot, J., Willis, J., Wu, X., Larsen, C., Rignot, E.,  
463 Muellerschoen, R., & Khazendar, A. (2019). Validation of Glacier Topographic

464 Acquisitions from an Airborne Single-Pass Interferometer. *Sensors*, 19(17), 3700.  
465 <https://doi.org/10.3390/s19173700>

466 Moller, D., Hensley, S., Sadowy, G., Fisher, C., Michel, T., Zawadzki, M., & Rignot, E.  
467 (2011). The Glacier and Land Ice Surface Topography Interferometer: An  
468 Airborne Proof-of-Concept Demonstration of High-Precision Ka-Band Single-  
469 Pass Elevation Mapping. *Geoscience and Remote Sensing, IEEE Transactions*  
470 *On*, 49, 827–842. <https://doi.org/10.1109/TGRS.2010.2057254>

471 Moore, R. D., Fleming, S. W., Menounos, B., Wheate, R., Fountain, A., Stahl, K., Holm,  
472 K., & Jakob, M. (2009). Glacier change in western North America: Influences on  
473 hydrology, geomorphic hazards and water quality. *Hydrological Processes*, 23(1),  
474 42–61. <https://doi.org/10.1002/hyp.7162>

475 Mouginot, J., Rignot, E., Bjørk, A. A., van den Broeke, M., Millan, R., Morlighem, M.,  
476 Noël, B., Scheuchl, B., & Wood, M. (2019). Forty-six years of Greenland Ice  
477 Sheet mass balance from 1972 to 2018. *Proceedings of the National Academy of*  
478 *Sciences*, 116(19), 9239–9244. <https://doi.org/10.1073/pnas.1904242116>

479 Ohlschlager, J. G. (2015). *Glacier Change on the Three Sisters Volcanoes, Oregon:*  
480 *1900–2010* [ProQuest Dissertations Publishing].  
481 <https://search.proquest.com/docview/1718552424?pq-origsite=primo>

482 O’Neal, M. A., Hanson, B., Carisio, S., & Satinsky, A. (2015). Detecting recent changes  
483 in the areal extent of North Cascades glaciers, USA. *Quaternary Research*, 84(2),  
484 151–158. <https://doi.org/10.1016/j.yqres.2015.05.007>

485 O’Neel, S., McNeil, C., Sass, L. C., Florentine, C., Baker, E. H., Peitzsch, E., McGrath,  
486 D., Fountain, A. G., & Fagre, D. (2019). Reanalysis of the US Geological Survey  
487 Benchmark Glaciers: Long-term insight into climate forcing of glacier mass  
488 balance. *Journal of Glaciology*, 65(253), 850–866.  
489 <https://doi.org/10.1017/jog.2019.66>

490 Ostrem, G., & Brugman, M. (1991). *Glacier mass balance measurements: A manual for*  
491 *field and office work* (Science Report No. 4; p. 224). National Hydrology  
492 Research Institute,.

493 Paul, F. (2008). Calculation of glacier elevation changes with SRTM: Is there an  
494 elevation-dependent bias? *Journal of Glaciology*, *54*(188), 945–946.

495 Pfeffer, W. T., Arendt, A. A., Bliss, A., Bolch, T., Cogley, J. G., Gardner, A. S., Hagen,  
496 J.-O., Hock, R., Kaser, G., & Kienholz, C. (2014). The Randolph Glacier  
497 Inventory: A globally complete inventory of glaciers. *Journal of Glaciology*,  
498 *60*(221), 537–552. <https://doi.org/10.3189/2014JoG13J176>

499 Rees, W. G. (2000). Technical note: Simple masks for shadowing and highlighting in  
500 SAR images. *International Journal of Remote Sensing*, *21*(11), 2145–2152.  
501 <https://doi.org/10.1080/01431160050029477>

502 Rosen, P. A., Hensley, S., Joughin, I. R., Li, F. K., Madsen, S. N., Rodriguez, E., &  
503 Goldstein, R. M. (2000). Synthetic aperture radar interferometry. *Proceedings of*  
504 *the IEEE*, *88*(3), 333–382. <https://doi.org/10.1109/5.838084>

505 Schumann, G. J.-P., Moller, D. K., & Mentgen, F. (2016). High-Accuracy Elevation Data  
506 at Large Scales from Airborne Single-Pass SAR Interferometry. *Frontiers in*  
507 *Earth Science*, *3*. <https://doi.org/10.3389/feart.2015.00088>

508 Shepherd, A., Ivins, E., Rignot, E., Smith, B., Van Den Broeke, M., Velicogna, I.,  
509 Whitehouse, P., Briggs, K., Joughin, I., & Krinner, G. (2018). Mass balance of the  
510 Antarctic Ice Sheet from 1992 to 2017. *Nature*, *558*, 219–222.

511 Sisson, T. W., Robinson, J. E., & Swinney, D. D. (2011). Whole-edifice ice volume  
512 change AD 1970 to 2007/2008 at Mount Rainier, Washington, based on LiDAR  
513 surveying. *Geology*, *39*(7), 639–642.

514 Surazakov, A. B., & Aizen, V. B. (2006). Estimating volume change of mountain glaciers  
515 using SRTM and map-based topographic data. *IEEE Transactions on Geoscience*  
516 *and Remote Sensing*, *44*(10), 2991–2995.

517 Zemp, M., Huss, M., Thibert, E., Eckert, N., McNabb, R., Huber, J., Barandun, M.,  
518 Machguth, H., Nussbaumer, S. U., Gärtner-Roer, I., Thomson, L., Paul, F.,  
519 Maussion, F., Kutuzov, S., & Cogley, J. G. (2019). Global glacier mass changes  
520 and their contributions to sea-level rise from 1961 to 2016. *Nature*, *568*(7752),  
521 382–386. <https://doi.org/10.1038/s41586-019-1071-0>

522

523 **Supplementary Online Material**

524

525 To identify the date of each glacier DEM, the glacier outlines were combined with a  
526 shapefile of the NED metadata (<https://viewer.nationalmap.gov/basic>) in ArcGIS (ESRI,  
527 Inc.). The NED from non-USGS sources (Table SOM1) did not include metadata for the  
528 imagery date. In those cases, we used the dates listed on the map collars of the USGS  
529 1:24000 topographic maps. Often the same aerial photographs used to create the  
530 topographic maps were also used to derive the NED. Photography used to create the  
531 portion of the NED overlapping the GLISTIN surveys were flown between 1950-1993,  
532 with only two glaciers surveyed in 1950 (Wind River Range, WY) and nine after 1990  
533 (Sierra Nevada, CA). There were 108 glacier outlines where the NED was derived from  
534 imagery spanning multiple years, of which 23 had USGS metadata, clearly identifying  
535 which portion of the outline corresponds with which year. The DEMs covering the  
536 remaining 85 glaciers were from non-USGS sources, and it is unclear what portion of the  
537 glacier were covered by imagery from which year. For G&PS, where multiple images  
538 were used to create the NED, if >80% of the G&PS area was imaged within a single year  
539 (21 G&PS), that year defined the date. For the remaining 64 G&PS, the date is defined as  
540 the average of all years listed. The reported RMSE of the NED (1999 version) is 3.74 m,  
541 but that RMSE under samples high elevation and slopes, fewer than ten samples for slope  
542 > 30°, and ~20 samples for elevations > 3000 m (Gesch, 2007). Therefore, the error over  
543 glaciers and the surrounding alpine environment is probably much higher.

544

545 The NED was split into regions corresponding to the mountain ranges covered by  
546 GLISTIN. In some cases, regions were split into smaller sub-regions to reduce processing  
547 time. Each was converted to the same vertical reference system as GLISTIN (WGS84)  
548 using Vdatum then projected into the UTM coordinate system and resampled to 10 m  
549 using bilinear interpolation. The pixel resolution was resampled to 10 m so that it was  
550 standard across all regions. Before resampling, the pixel resolution of the NED differed  
551 by region, ranging from 8.5 m (northern Cascades, WA) to 9.4 m (Sierra Nevada, CA).  
552 GLISTIN was also resampled to 10 m and co-registered to the NED using the methods of

553 Berthier et al. (2007). The co-registration process reduces the horizontal and vertical  
554 offsets between the DEMs by first minimizing the standard deviation of differences over  
555 control zones and then applying that shift to the whole DEM. Offsets between DEMs can  
556 significantly influence estimates of elevation change, particularly on steep slopes  
557 (Berthier et al., 2007).

558

559

560

561

562

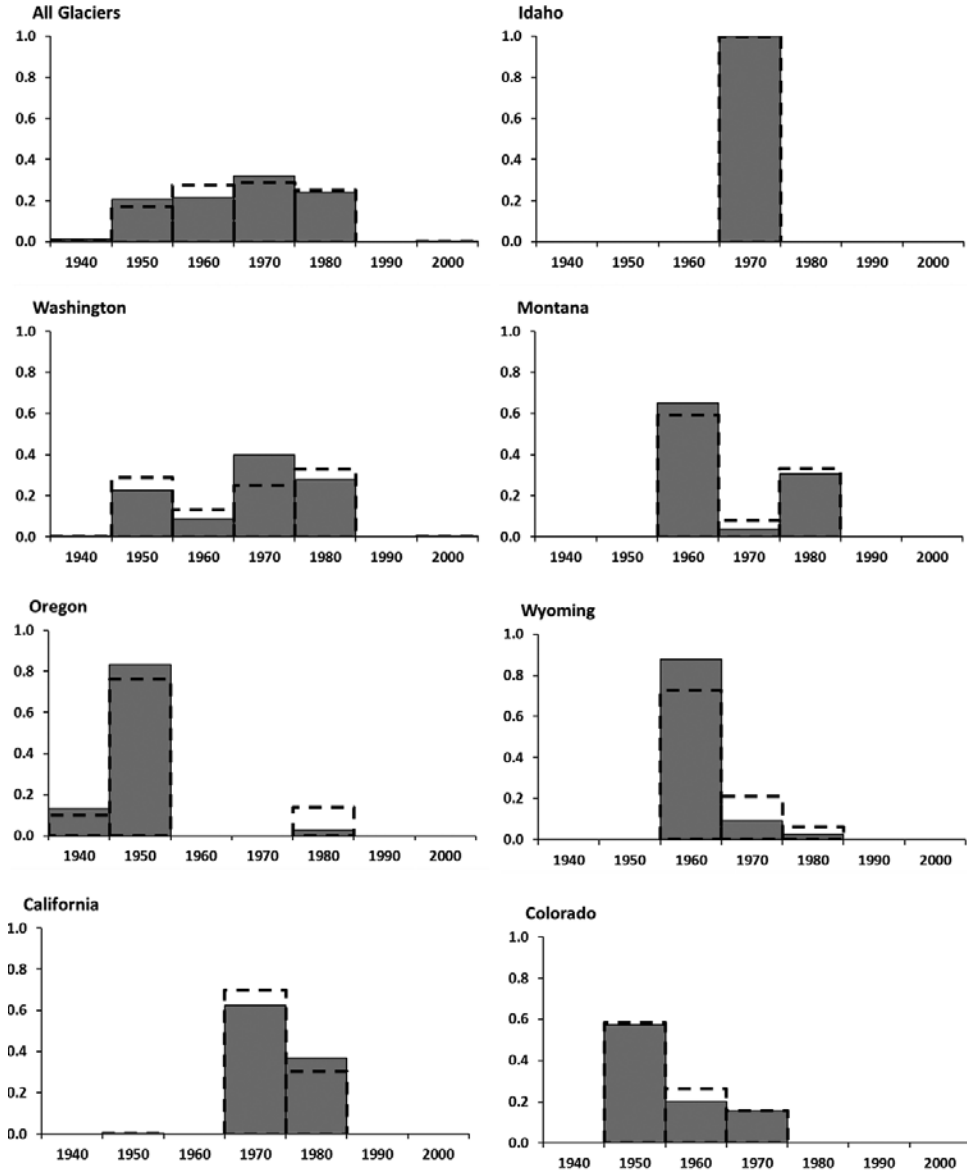
563

564

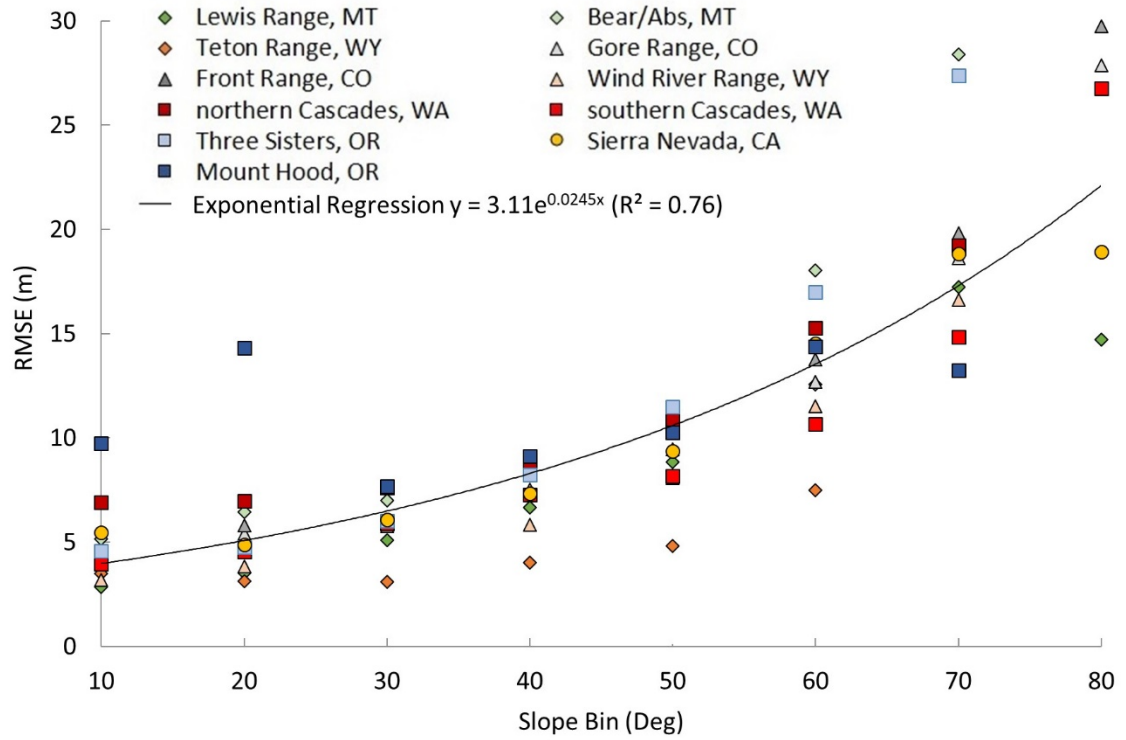
565

566

567



568  
 569 **Figure SOM1.** Acquisition dates for imagery used to create the U.S. Geological Survey  
 570 1:24000 topographic maps for areas with glaciers and perennial snowfields (G&PS). The  
 571 date on the x-axis represents the full decade (e.g., 1960 = 1960 to 1969). The y-axis is the  
 572 fraction of the total. The solid grey bars are the fraction of area, and the dashed outline is  
 573 the fraction of the number of G&PS. The top left depicts the imagery for all G&PS in the  
 574 western U.S. The other graphs show the acquisition date for each state. Reprinted from  
 575 Fountain et al. (2017).  
 576



578

579 **Figure SOM2.** Root mean square error (RMSE) between GLISTIN elevations and the  
 580 National Elevation Dataset for control zones binned by 10° slopes. The slope label  
 581 represents the maximum of that bin. The 10° slope bin includes slopes of 0°.

582

583

584

585

586

587

588

589

590

591

592

593 **Table SOM1.** List of sources compiled for the historical elevation data. The three  
 594 sources used were the National Map, maintained by the U.S. Geological Survey (USGS),  
 595 the Oregon office of the Bureau of Land Management (BLM), and the Geomorphological  
 596 Research Group at the University of Washington (UW).  
 597

State/Range	Source	Website
<b>California</b>		
Sierra Nevada	USGS	<a href="https://viewer.nationalmap.gov/basic">https://viewer.nationalmap.gov/basic</a>
<b>Colorado</b>		
Front	USGS	<a href="https://viewer.nationalmap.gov/basic">https://viewer.nationalmap.gov/basic</a>
Gore	USGS	<a href="https://viewer.nationalmap.gov/basic">https://viewer.nationalmap.gov/basic</a>
<b>Montana</b>		
Beartooth-Absaroka	USGS	<a href="https://viewer.nationalmap.gov/basic">https://viewer.nationalmap.gov/basic</a>
Lewis	USGS	<a href="https://viewer.nationalmap.gov/basic">https://viewer.nationalmap.gov/basic</a>
<b>Oregon</b>		
Cascade	BLM	<a href="http://earthexplorer.usgs.gov">http://earthexplorer.usgs.gov</a>
<b>Washington</b>		
northern Cascades	UW	<a href="http://gis.ess.washington.edu/data/">http://gis.ess.washington.edu/data/</a>
northern Cascades	USGS	<a href="https://viewer.nationalmap.gov/basic">https://viewer.nationalmap.gov/basic</a>
southern Cascades	BLM	<a href="http://earthexplorer.usgs.gov">http://earthexplorer.usgs.gov</a>
<b>Wyoming</b>		
Teton	USGS	<a href="https://viewer.nationalmap.gov/basic">https://viewer.nationalmap.gov/basic</a>
Wind River	USGS	<a href="https://viewer.nationalmap.gov/basic">https://viewer.nationalmap.gov/basic</a>

598  
 599  
 600  
 601  
  
 602  
  
 603  
  
 604  
  
 605  
  
 606  
 607



608 **Table SOM2.** List of lidar datasets used for the absolute error assessment. The datasets  
 609 came from three sources, the National Map, maintained by the U.S. Geological Survey  
 610 (USGS; <https://viewer.nationalmap.gov/basic/>), Washington Department of Natural  
 611 Resources (WA DNR; <https://lidarportal.dnr.wa.gov/>), and Oregon Department of  
 612 Geology and Mineral Industries (DOGAMI;  
 613 <https://gis.dogami.oregon.gov/maps/lidarviewer/>). ‘Uncertainty’ refers to the reported  
 614 absolute vertical uncertainty of the lidar.

<u>Region</u>	<u>Year</u>	<u>Source</u>	<u>Uncertainty</u>
Mount Adams, WA	2016	USGS	0.07
northern Cascade Range, WA	2009	WA DNR	0.04
Mount Rainier, WA	2007/2008	WA DNR	0.04
Three Sisters, OR	2010	DOGAMI	0.04

615  
 616  
 617  
 618  
 619

620 **Table SOM3.** Amount of missing data in GLISTIN mosaic based on the number of flight  
 621 passes. ‘Missing Area’ is the total area of pixels for the listed category in the GLISTIN  
 622 mosaic that had no elevation data. ‘Total Area’ is the total area of all pixels for the  
 623 category in the GLISTIN mosaic. ‘% Missing’ is the ratio of the missing area divided by  
 624 the total area within that category.

625

<u>Flight Passes</u>	<u>Missing Area (km<sup>2</sup>)</u>	<u>Total Area (km<sup>2</sup>)</u>	<u>% Missing</u>
1	8575.94	10259.58	83.59
2	5368.17	15877.95	33.81
3	1167.58	7344.92	15.90
4	912.02	6511.64	14.01
5	154.29	813.70	18.96
6	51.56	379.55	13.59
7	8.67	147.40	5.88
8	4.00	64.31	6.23

626  
 627  
 628  
 629  
 630

631 **Table SOM4.** Elevation uncertainty for control zones estimated from comparing  
632 GLISTIN, lidar, and National Elevation Dataset (NED). The sources and accuracy of the  
633 lidar data are listed in the supplementary online material. ‘Region’ refers to the region of  
634 the mosaicked GLISTIN digital elevation models, ‘Area’ is the area of the control zone,  
635 ‘Swath Count’ is a range of the number of GLISTIN flights covering the control zones,  
636 and standard deviation, ‘RMSE’ is the root mean square error. The ‘All’ column  
637 combines data from the three regions (columns to the left) with multiple GLISTIN  
638 passes.

	northern Cascades, WA	Mount Rainier, WA	Three Sisters, OR	All	Mount Adams, WA
Lidar Year	2009	2007/08	2010	---	2016
Area (km <sup>2</sup> )	1.61	3.10	1.95	6.66	12.74
Swath Count	3-6	3-4	2	2-6	1
<b>GLISTIN minus lidar</b>					
RMSE (m)	+1.79	+1.87	+1.64	+1.78	+3.20
Mean ± std (m)	-0.14 ± 1.78	+0.38 ± 1.83	+0.10 ± 1.63	+0.17 ± 1.78	0.00 ± 3.20
Median (m)	-0.08	+0.17	+0.15	+0.11	0.00
<b>GLISTIN minus NED</b>					
RMSE (m)	+8.84	+3.36	+7.14	+6.46	+6.22
Mean ± std (m)	+4.49 ± 7.61	+0.57 ± 3.31	-2.05 ± 6.84	+1.05 ± 6.38	+0.49 ± 6.20
Median (m)	+4.83	+035	-0.49	+0.80	+0.52
<b>Lidar minus NED</b>					
RMSE (m)	+7.21	+2.27	+8.37	+5.89	+5.60
Mean ± std (m)	+0.13 ± 7.21	-0.21 ± 2.27	-2.87 ± 7.86	-0.89 ± 5.83	-0.18 ± 5.60
Median (m)	+0.54	-0.15	-0.62	-0.19	-0.03

639  
640  
641  
642  
643  
644  
645  
646

647 **Table SOM5.** Root mean square error (RMSE), and mean elevation difference between  
 648 the National Elevation Dataset and GLISTIN derived elevations of barren earth control  
 649 zones, and total area (Area) of the barren earth control zones in each region sampled.

<b>Region</b>	<b>RMSE (m)</b>	<b>Mean ± std (m)</b>	<b>Area (km<sup>2</sup>)</b>
northern Cascades, WA	7.74	+0.33 ± 7.73	107.34
southern Cascades, WA	5.81	+0.62 ± 5.83	27.06
Mount Hood, OR	8.26	-2.42 ± 8.25	10.21
Three Sisters, OR	6.07	+0.64 ± 6.03	23.19
Sierra Nevada, CA	6.64	-1.72 ± 6.42	191.16
Lewis, MT	8.89	+1.72 ± 8.80	22.16
Beartooth-Absaroka, MT	10.57	-0.26 ± 10.57	7.83
Teton, WY	3.53	-0.32 ± 3.52	0.93
Wind River, WY	6.55	-0.96 ± 6.48	7.81
Front, CO	8.31	+1.40 ± 8.19	36.54
Gore, CO	8.15	+1.68 ± 7.98	27.43
<b>Total</b>	<b>7.32</b>	<b>-0.37 ± 7.31</b>	<b>461.67</b>

650  
 651  
 652  
 653  
 654  
 655  
 656  
 657  
 658  
 659  
 660  
 661  
 662  
 663  
 664

665 **Table SOM6.** Volume change estimates for glaciers and perennial snowfields in select  
666 regions and periods. Volume change was estimated between the initial NED year and the  
667 GLISTIN year of 2016 for glaciers and perennial snowfields with  $\geq 80\%$  GLISTIN. The  
668 change was grouped by region and year. The year listed is the last in the 5-year interval  
669 (e.g., 1955 = 1951 to 1955). ‘Num’ is the number of G&PS for that category.  
670

Region/Year/Type	Num	Area (km <sup>2</sup> )	Volume Change (m <sup>3</sup> x 10 <sup>6</sup> )	Specific Vol Change (m)	Specific Vol Change Rate (m yr <sup>-1</sup> )
<b>WA Cascades</b>					
1960	75	19.70	-336.81 ± 117.49	-17.10 ± 5.96	-0.31 ± 0.11
Glacier	29	17.75	-312.42 ± 106.56	-17.60 ± 6.00	-0.31 ± 0.11
Snowfield	46	1.95	-24.40 ± 10.93	-12.48 ± 5.59	-0.22 ± 0.10
1970	53	53.36	-507.94 ± 255.44	-9.52 ± 4.79	-0.21 ± 0.10
Glacier	23	52.40	-501.59 ± 250.65	-9.57 ± 4.78	-0.21 ± 0.10
Snowfield	30	0.96	-6.35 ± 4.79	-6.62 ± 5.00	-0.14 ± 0.11
1975	82	15.88	-290.34 ± 124.61	-18.29 ± 7.85	-0.45 ± 0.19
Glacier	24	13.14	-249.19 ± 102.35	-18.96 ± 7.79	-0.46 ± 0.19
Snowfield	58	2.73	-41.16 ± 22.26	-15.05 ± 8.14	-0.37 ± 0.20
1980	20	21.40	-320.08 ± 180.75	-14.95 ± 8.44	-0.42 ± 0.23
Glacier	8	20.81	-309.81 ± 175.82	-14.89 ± 8.45	-0.41 ± 0.23
Snowfield	12	0.59	-10.27 ± 4.94	-17.32 ± 8.33	-0.48 ± 0.23
1985	101	34.14	-662.12 ± 275.94	-19.39 ± 8.08	-0.63 ± 0.26
Glacier	40	31.54	-628.40 ± 257.10	-19.92 ± 8.15	-0.64 ± 0.26
Snowfield	61	2.60	-33.71 ± 18.83	-12.97 ± 7.25	-0.42 ± 0.23
<b>OR Cascades</b>					
1960	44	14.47	-215.07 ± 90.29	-14.86 ± 6.24	-0.27 ± 0.11
Glacier	13	12.19	-188.44 ± 76.15	-15.46 ± 6.25	-0.28 ± 0.11
Snowfield	31	2.28	-26.63 ± 14.14	-11.67 ± 6.19	-0.21 ± 0.11
1975	25	8.09	-143.32 ± 50.91	-17.71 ± 6.29	-0.43 ± 0.15
Glacier	9	7.44	-137.50 ± 46.93	-18.48 ± 6.31	-0.45 ± 0.15
Snowfield	16	0.65	-5.83 ± 3.98	-8.97 ± 6.13	-0.22 ± 0.15
<b>Sierra Nevada</b>					
1975	16	0.39	-4.19 ± 2.38	-10.74 ± 6.09	-0.26 ± 0.15
Glacier	2	0.13	-1.85 ± 0.73	-14.57 ± 5.73	-0.36 ± 0.14
Snowfield	14	0.26	-2.35 ± 1.65	-8.90 ± 6.26	-0.22 ± 0.15
1980	35	2.61	-42.98 ± 18.44	-16.44 ± 7.05	-0.46 ± 0.20
Glacier	12	1.95	-34.69 ± 13.74	-17.76 ± 7.04	-0.49 ± 0.20
Snowfield	23	0.66	-8.30 ± 4.70	-12.55 ± 7.10	-0.35 ± 0.20
1985	109	3.87	-40.62 ± 18.78	-10.50 ± 4.86	-0.34 ± 0.16
Glacier	9	1.40	-19.27 ± 8.63	-13.79 ± 6.18	-0.44 ± 0.20
Snowfield	100	2.47	-21.35 ± 10.15	-8.64 ± 4.11	-0.28 ± 0.13
<b>Wind River</b>					
1970	64	23.95	-365.80 ± 115.43	-15.28 ± 4.82	-0.33 ± 0.10
Glacier	19	21.17	-345.41 ± 102.55	-16.31 ± 4.84	-0.35 ± 0.11
Snowfield	45	2.77	-20.40 ± 12.89	-7.35 ± 4.64	-0.16 ± 0.10

1975	24	0.60	$-3.61 \pm$	2.82	$-6.01 \pm 4.70$	$-0.15 \pm 0.11$
Glacier	1	0.05	$-1.12 \pm$	0.27	$-20.90 \pm 4.96$	$-0.51 \pm 0.12$
Snowfield	23	0.55	$-2.49 \pm$	2.56	$-4.55 \pm 4.68$	$-0.11 \pm 0.11$

671  
672  
673